THE UNIVERSITY OF MICHIGAN

COLLEGE OF ENGINEERING
Department of Engineering Mechanics
Department of Mechanical Engineering

Tire and Suspension Systems Research Group

Technical Report No. 19

AN ANALOG FOR THE ROLLING PNEUMATIC TIRE UNDER LOAD

S. K. Clark

Project Director: S. K. Clark

ORA Project 02957

enem

UMR12UY

The Tire and Suspension Systems Research Group
at The University of Michigan is sponsored by:

TABLE OF CONTENTS

LIST OF FIGURES

NOMENCLATURE

English Letters

a   Undeformed radius of the cylindrical shell, a structural radius measured to the midline of the shell thickness

a_o Undeformed geometric radius of the cylindrical shell, measured to the outside surface of the shell.

A,B,C,D   Constants of integration

b_F, b_A Wave numbers for motion forward and aft of the contact patch, respectively

b_W Width of cylindrical shell. This would normally correspond approximately to the tread width of a tire.

c   Viscous damping coefficient

c_1 Propagation velocity $\sqrt{E/p}$

$\bar{c}$ Dimensionless viscous damping coefficient

CWA   Dimensionless damping factor

d   Real part of complex root

$\bar{D}$ $E \cdot h$ (for a narrow shell or ring)

e   Base of natural logarithms

E   Young's modulus of shell material

g   Damping constant used in hysteresis damping

h   Shell thickness

H   Shell deflection against a plane

i $\sqrt{-1}$

k   Elastic stiffness of shell internal foundation

K $Eh^3/12$ (for a narrow shell or ring)

KA   Dimensionless spring rate

MO   Moment about axle

N,M   Shell stress resultants

p   Pressure

p_O Internal pressure

$p(\theta)$ External pressure

P   Vertical load carried by shell

PA   Dimensionless internal pressure

PE   Dimensionless external pressure

PO   Dimensionless internal pressure

PQ   Dimensionless external pressure

q   Complex root

Q   Shear force, lbs

t   Time

u,v,w   Shell displacements

WA   Dimensionless angular velocity

$z,\bar{z}$ Dimensionless shell deflection w/a.

Greek Letters

α^2 $h^2/12a^2$, a dimensionless constant

μ Poisson's ratio

ρ Material density in shell

Ω Shell angular velocity

$\overline{\Omega}$ Dimensionless shell angular velocity

τ Dimensionless time

Θ_1 $\Theta - \Omega t$, a moving co-ordinate

Θ_A, Θ_F Angular positions of edge of contact patch, aft and forward directions respectively

I. INTRODUCTION

It is a reasonably good approximation to state that most pneumatic tire problems can be separated into two groups, these being:

(a) Those involving motion in the plane of the wheel or rim;

(b) Those involving motion transverse to the plane of the wheel or rim. There are, of course, occasional exceptions to this compartmentalization but in the main it is felt that considerable knowledge could be gained by developing methods for analytically studying pneumatic tire performance either in the plane of the wheel or transverse to the plane of the wheel.

Preliminary efforts have been made by such writers as Saito[1] and Thorsen[2] in developing techniques for predicting cornering forces and other effects transverse to the plane of the wheel. To the best of the writer's knowledge, no systematic attempts have been made to study motion in the plane of the wheel prior to Ref. 3, issued by this group. In that report, the use of an elastically supported cylindrical shell was proposed as a means for studying the static loading of a pneumatic tire against an infinitely rigid, frictionless plane. The results obtained from that analysis seemed to agree fairly well with contact patch length measurements made on real pneumatic tires.

In view of the many current problems associated with pneumatic tire motion in the plane of the wheel, it was felt desirable to attempt to extend these analytical techniques to those dynamic cases which can be profitably studied.

1

II. SUMMARY

An elastically supported cylindrical shell is used as a model for the dynamic rolling of a loaded pneumatic tire. Such a model includes many of the effects found in the real tire, such as bending of the tread in the contact patch region, elastic support coming from the inflated sidewalls and loss effects coming from the inherent dissipative properties of the materials used.

Methods are presented for calculating the dynamic contact patch areas of such a model, and it is shown that these are influenced considerably by rolling velocity, the constructional parameters of the tire and its loss characteristics. Dynamic pressure distributions inside these contact patch areas may also be obtained analytically, and techniques are given for doing this.

The free motion of the penumatic tire outside of the contact patch region is of considerable importance in the study of standing wave phenomena in tires. Techniques are developed for calculating the radial deflection of a rolling pneumatic tire both forward and aft of its contact patch region, and such calculations generally agree with the type of phenomena which are observed.

As examples of the use of such a model, an elastically supported cylindrical shell with both a viscous loss and hysteresis loss law are used as a basis for the calculation of the load carrying and drag proper-

ties of a real pneumatic tire, to the extent that the various tire properties may be approximated. In addition, results are given in which the predicted performance of bias ply tires is compared to that of belted tires.

Many of the technically important characteristics of this model depend on the specific mathematical form of the loss mechanism included in the system. These are probably best known to those who have access to considerable quantities of test information on rubber properties, and no attempt is made in this report to explore this subject.

III. THE BASIC DYNAMIC MODEL FOR A ROLLING TIRE.

We consider first a generalized cylindrical shell under arbitrary loads. This is shown in Figure 1, taken from Flugge.[4]
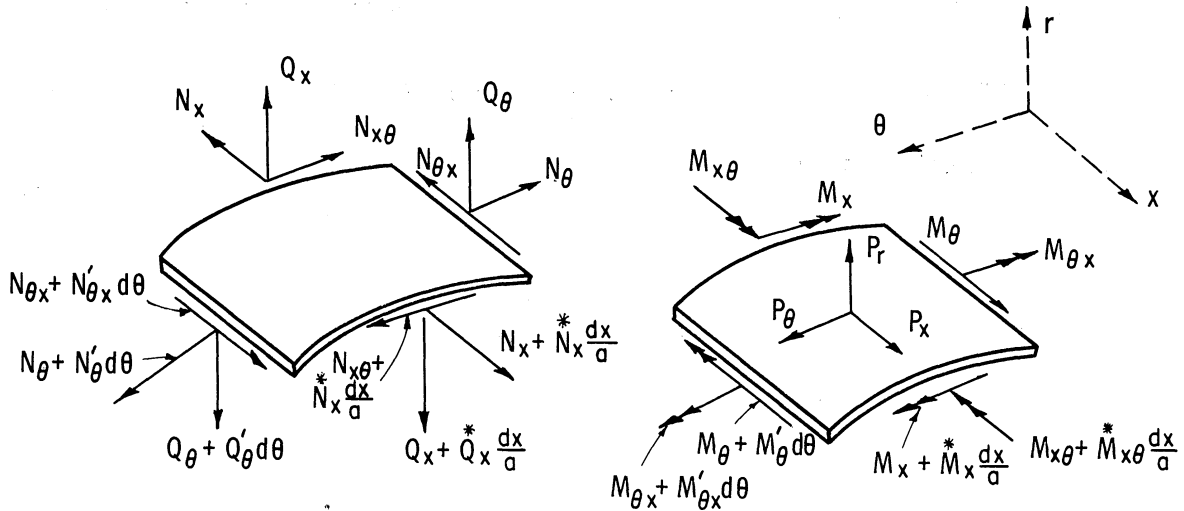

Figure 1. Shell stress resultant conventions and nomenclature.

From Figure 1, force equilibrium equations may be written for the element of cylindrical shell surface. Generally, these equations are directed in the x, and r directions, and are given as:

$$\overset{*}{N}_x + N'_{\theta x} + P_x \cdot a = 0$$

$$a\, N'_\theta + a\, \overset{*}{N}_{x\theta} - M'_\theta - \overset{*}{M}_{x\theta} + P_\theta\, a^2 = 0 \tag{1}$$

$$M''_\theta + \overset{*}{M}'_{x\theta} + \overset{*}{M}'_{\theta x} + \overset{**}{M}_x + a N_\theta - P_r\, a^2 = 0$$

The following symbols are used:

$$a\, \frac{\partial (\ )}{\partial x} = (\ \overset{*}{)}\qquad \frac{\partial (\ )}{\partial \theta} = (\ )' \tag{2}$$

It is next necessary to consider displacements of a cylindrical shell, where we let

> u = displacement along the generator, positive in the direction of increasing x;

> v = displacement along a circle of radius a, positive in direction of increasing Θ;

> w = radial displacement, positive outward.

Using this notation, and assuming that: (1) all points lying on one normal to the middle surface before deformation do the same after deformation; (2) that for all kinematic relations the distance z of a point from the middle surface may be considered as unaffected by the deformations of the shell; (3) that the stress σ_r may be considered negligible compared with the stresses σ_x and σ_Θ.

By use of such assumptions, and by consideration of the definitions of shell forces, one may finally express the various shell forces and moments in terms of the deformation by means of the equations

$$N_\Theta = \frac{\overline{D}}{a}(v'+w+\mu\overset{*}{u}) + \frac{K}{a^3}(w+w'')$$

$$N_x = \frac{\overline{D}}{a}(\overset{*}{u}+\mu v'+\mu w) - \frac{K}{a^3}\overset{**}{w}$$

$$N_{\Theta x} = \frac{\overline{D}}{a}\cdot\frac{1-\mu}{2}(u'+\overset{*}{v}) + \frac{K}{a^3}\cdot\frac{1-\mu}{2}(u'+\overset{*}{w}') \qquad (3)$$

$$N_{x\Theta} = \frac{\overline{D}}{a}\cdot\frac{1-\mu}{2}(u'+\overset{*}{v}) + \frac{K}{a^3}\cdot\frac{1-\mu}{2}(\overset{*}{v}-\overset{*}{w}')$$

$$M_\Theta = \frac{K}{a^2}(w+w''+\mu\overset{**}{w})$$

$$M_x = \frac{K}{a^2}(\overset{**}{w}+\mu w''-\overset{*}{u}-\mu v')$$

5

$$M_{\Theta x} = \frac{K}{a^2}(1-\mu)\left(\overset{*}{w}' + \frac{u'}{2} - \frac{\overset{*}{v}}{2}\right)$$

$$M_{x\Theta} = \frac{K}{a^2}(1-\mu)\left(\overset{*}{w}' - \overset{*}{v}\right)$$

If one uses Eqs. (3) and substitutes them into Eqs. (1), it is possible to obtain the three equations of equilibrium in terms of the three differential equations in displacements u, v and w of the middle surface of the shell. These equations become

$$\overset{**}{u} + \frac{1-\mu}{2}u'' + \frac{1+\mu}{2}\overset{*}{v}' + \mu\overset{*}{w} + \alpha^2[\frac{1-\mu}{2}u'' - \overset{***}{w} + \frac{1-\mu}{2}\overset{*}{w}''] + \frac{pxa^2}{D} = 0$$

$$(\frac{1+\mu}{2})\overset{*}{u}' + v'' + \frac{1-\mu}{2}\overset{**}{v} + w' + \alpha^2[\frac{3}{2}(1-\mu)\overset{**}{v} - \frac{3-\mu}{2}\overset{**}{w}'] + \frac{P\Theta a^2}{D} = 0$$

$$\text{(3)}$$

$$\mu\overset{*}{u} + v' + w + \alpha^2[\frac{1-\mu}{2}\overset{*}{u}'' - \overset{***}{u} - \frac{3-\mu}{2}\overset{**}{v}' + \overset{****}{w} + 2\overset{**}{w}'' + w''''$$

$$\text{(4)}$$

$$+ 2w'' + w] - \frac{Pr\,a^2}{D} = 0$$

We next wish to consider the specific case of a rather narrow cylindrical shell which has no variation of loading with respect to the x direction. In this case, the shell takes on the form shown in Figure 2, where a rather narrow shell of width b_w and thickness h is made of material of modulus E and density ρ, the radius of the cylinder being a.
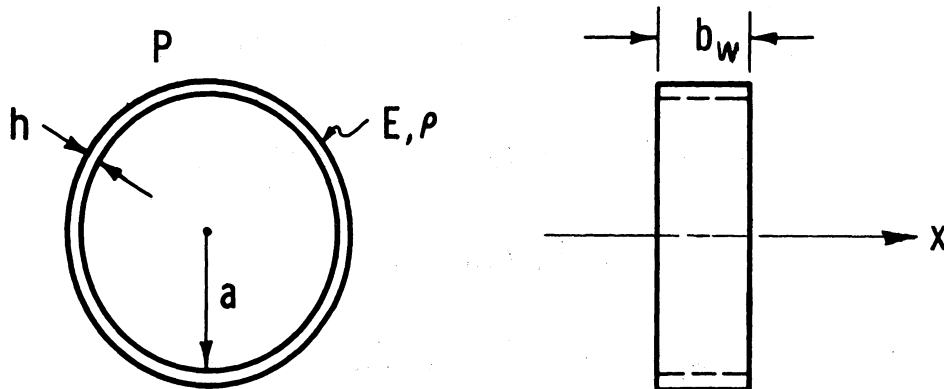

Figure 2. Narrow cylindrical shell notation.

If the loading is uniform with respect to the x direction, and if the width b_w is small enough so that contraction in the x direction may be neglected, than one may visualize that all derivatives with respect to x in Eqs. (4) will vanish. In addition, all displacements u in the x direction become negligible and will be dropped, as will pressure components in the x direction. Allowing thse simplifying assumptions to be used in Eqs. (4) causes them to reduce to

$$\frac{\partial}{\partial\Theta} \left(\frac{\partial v}{\partial\Theta} + w\right) + P_\Theta \frac{a^2}{D} = 0$$

$$\left(\frac{\partial v}{\partial\Theta} + w\right) + \alpha^2 \left[\frac{\partial^4 w}{\partial\Theta^4} + 2\frac{\partial^2 w}{\partial\Theta^2} + w\right] - \frac{Pr^a}{D} = 0$$

(5)

There are several ways that one may proceed to analyze Eqs. (5). Perhaps the simplest of these is to visualize that for a frictionless plane p_Θ vanishes so that the first of Eqs. (5) simply states that

$$\left(\frac{\partial v}{\partial\Theta} + w\right) = \text{Cons't} \tag{6}$$

We may arbitrarily set the value of the constant in Eq. (6) equal to zero, in which case the pair of Eqs. (5) reduce immediately to the single equation

$$\alpha^2 (w^{IV} + 2 w'' + w) = \frac{Pr^{a^2}}{Eh} \tag{7}$$

This equation now represents the equation for deflection of a cylindrical shell against a frictionless load, so that only radial pressures exist. Note that the constant α^2 is given by

$$\alpha^2 = \frac{h^2}{12a^2}$$

In Eq. (7), it is desirable to include most of the properties of a real pneumatic tire by means of adjusting the radial pressure term p_r for various tire effects. Specifically, it is desired to support the elastic shell by means of some kind of generalized impedance in such a way that both real elastic moduli and imaginary elastic moduli can be operative. This might be thought of, in some respects, as filling the inside of the shell with a massless foam-like material of generalized impedance. For purposes of this report, the generalized impedance will be specialized to the specific case of a real elastic and viscous loss support system, but it is readily understood that the viscous loss support mechanism may be replaced by other mechanisms such as a hysteresis type of loss. This is done in one of the example problems worked out in the last section of this report. For the present, the viscous loss mechanism represents a very simple device which is easily treated analytically, and for that reason will be retained here.

As an additional feature of Eq. (7), it is desirable to include both a uniform internal inflation pressure and an external pressure loading term denoting contact pressures coming from contact with the ground surface.

Finally, inertia terms form part of the radial loading since it may be anticipated that the shell in question will be accelerating in the w direction as well as being subjected to an overall rigid body rotation of angular velocity Ω. Accounting for all of these factors, one may write the total radial pressure of the shell in the form

8

(a) $p_r = -\rho h[\ddot{w}-(a+w)\Omega^2]$

(b) $p_r = -kw$

(c) $p_r = c\dot{w}$

(d) $p_r = p_0$ (8)

(e) $p_r = -p(\Theta)$

where

$$\frac{\partial(\ )}{\partial t} = (\dot{\ })$$

Including all of these effects into Eq. (7), one finally obtains

$$\frac{a^2\ddot{w}}{c_1^2} + \frac{a^2c}{Eh}\dot{w} + \alpha^2 w^{IV} + 2\alpha^2 w''$$

$$+ w[\alpha^2 + \frac{ka^2}{Eh} - \frac{\Omega^2 a^2}{c_1^2}] = \frac{a^2}{Eh}[p_0 - p(\Theta) + \rho h a \Omega^2] \qquad (9)$$

In this equation, the presence of the Ω^2 term is due to the fact that the shell is assumed to be rotating with angular velocity Ω. We will next allow loads to move in the opposite direction to Ω around the periphery of the rotating shell by means of transforming the shell equations into a new independent variable

$$\Theta_1 = \Theta - \Omega t$$

$$\frac{\partial(\ )}{\partial t} = \frac{\partial(\ )}{\partial t} - \Omega \frac{\partial(\ )}{\partial \Theta_1} \qquad (10)$$

$$\frac{\partial^2(\ )}{\partial t^2} = (\ddot{\ }) - 2\Omega(\dot{\ }) + \Omega^2(\ )''$$

Using these, one obtains

$$\frac{a^2}{c_1^2}(\Omega^2 w'' - 2\Omega \dot{w}' + \ddot{w}) + \frac{a^2c}{Eh}(\dot{w} - \Omega w') \qquad (11)$$

9

$$+\alpha^2 w^{IV} + 2\alpha^2 w'' + w[\alpha^2 + \frac{ka^2}{Eh} - \frac{\Omega^2 a^2}{c_1^2}] \tag{11}$$

$$= \frac{a^2}{Eh}[-p(\Theta) + p_0 + \rho ha\Omega^2]$$

where

$$c_1^2 = E/\rho$$

Next, introduce the new variables (see Ref. 5)

$$\frac{w}{a} = z \qquad \frac{tc_1}{a} = \tau \qquad c_1^2 = \frac{E}{\rho} \tag{12}$$

from which the equation of motion of the shell may now be written in the

form

$$\overset{\circ\circ}{z} + \frac{acc_1}{Eh}\overset{\circ}{z} - \frac{2a\Omega}{c_1}\overset{\circ}{z}' + \alpha^2 z^{IV}$$

$$+ (2\alpha^2 + \frac{a^2\Omega^2}{c_1^2})z'' - \frac{a^2 c\Omega}{Eh}z' \tag{13}$$

$$+ (\alpha^2 + \frac{ka^2}{Eh} - \frac{\Omega^2 a^2}{Eh})z = \frac{a}{Eh}[-p(\Theta) + p_0 + \rho ha\Omega^2]$$

Introducing the variable

$$\frac{\Omega a}{c_1} = \overline{\Omega} \tag{14}$$

one finally obtains Eq. (13) in the form

$$\overset{\circ\circ}{z} + \frac{acc_1}{Eh}\overset{\circ}{z} - 2\overline{\Omega}\overset{\circ}{z}' + \alpha^2 z^{IV} + (2\alpha^2 + \overline{\Omega}^2)z''$$

$$- \frac{acc_1}{Eh}\overline{\Omega}z' + (\alpha^2 + \frac{ka^2}{Eh} - \overline{\Omega}^2)z \tag{15}$$

$$= \frac{a}{Eh}[-p(\Theta) + p_0 + \rho ha\Omega^2]$$

In Eq. (15), we define the new constants as follows:

$$\frac{ac_1 c}{Eh} = \overline{c} \qquad \frac{a\ p(\Theta)}{Eh} = PE$$

$$\frac{ap_0}{Eh} = PO \tag{16}$$

10

and dividing by α^2, one finally obtains the equation of motion

$$\frac{\ddot{z}}{\alpha^2} + \frac{\bar{c}}{\alpha^2}\,\dot{z} - \frac{2\bar{\Omega}^2}{\alpha^2}\,\dot{z}' + z^{IV} + \left(2.+\frac{\bar{\Omega}^2}{\alpha^2}\right)z'' - \frac{\bar{c}\bar{\Omega}}{\alpha^2}\,z'$$

$$+ \left(1. + \frac{\bar{k}}{\alpha^2} - \frac{\bar{\Omega}^2}{\alpha^2}\right)z = -\frac{PE}{\alpha^2} + \frac{\bar{\Omega}^2}{\alpha^2} + \frac{PO}{\alpha^2} \qquad (17)$$

where

$$\bar{k} = \frac{ka^2}{Eh}$$

Equation (17) is an equation for motion of the cylindrical shell and contains all terms necessary for representing most of the phenomena which can be observed in a rolling pneumatic tire. Loss terms are represented through the viscous loss constant $\bar{c}$, dynamic terms through the quantity $\bar{\Omega}$ and elastic terms through the quantity $\bar{k}$. The angular velocity of the wheel is given by the dimensionless angular velocity $\bar{\Omega}$ so that Eq. (17) in effect represents a circular cylindrical shell, supported as indicated in Figure 3, with a moving load of angular velocity Ω. In addition to this angular velocity Ω, one may superimpose a rigid body rotation of angular velocity Ω in the opposite direction, as was done with the inertia term of the form $(a + w)\Omega^2$ in Eq. (8). This term, whose effect is to superimpose the rigid body rotation of angular velocity Ω on the entire system, results in Eq. (17) now representing rotating tire with stationary impressed load, such as is shown in Figure 3.
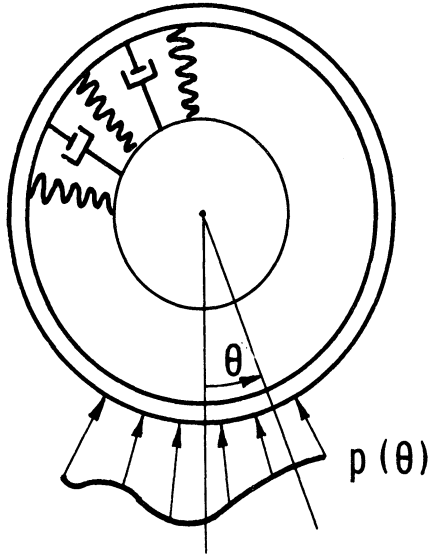
Figure 3. Shell characteristics.

We now consider steady state solutions to Eq. (17). Under this condition, all time derivatives vanish and making substitutions of constants in the form

$$\frac{\bar{\Omega}^2}{\alpha^2} = WA; \qquad \frac{\bar{c}\,\bar{\Omega}}{\alpha^2} = CWA; \qquad \frac{\bar{k}}{\alpha^2} = KA \qquad (18)$$

$$\frac{PE}{\alpha^2} = P\Theta \qquad \frac{PO}{\alpha^2} = PA$$

one sees that this reduces to

$$z^{IV} + (2 + WA)z'' - (CWA)z' + (1 + KA-WA)z$$

$$= PA - P\Theta + WA \qquad (19)$$

where, of course, the primes represent derivatives with respect to the variable Θ_1, and in general Eq. (19) represents steady state, or standing wave, solutions to the deformation of the rotating cylindrical shell.

First imagine the process of inflation only. Here, one may define a particular solution associated with the inflation of the static, or non-

12

rolling pneumatic wheel in which the constant WA vanishes. The particular solution becomes

$$z_p = \frac{PA}{1 + KA} \qquad (20)$$

This value of dimensionless displacement may be thought of as that associated with the inflation process. Now define the new variable

$$\bar{z} = z - z_p \qquad (21)$$

Using this variable, the equation of motion (19) becomes

$$\bar{z}^{IV} + (2+WA)\bar{z}'' - (CWA)\bar{z}' + (1+KA-WA)\bar{z}$$
$$- WA \left(1 + \frac{PA}{1+KA}\right) = -PQ \qquad (22)$$

Equation (22) now represents a working equation for the deformation of a cylindrical shell of the form being discussed, where dimensionless deflections $\bar{z}$ are now measured from the inflated position and not from the initial position. From Eq. (22) one may see that a static problem may readily be obtained by allowing the values WA and CWA both to vanish simultaneously. This allows Eq. (22) to reduce immediately to Eq. (23) as given below.

$$\bar{z}^{IV} + 2\bar{z}'' + (1+KA)\bar{z} = -PQ \qquad (23)$$

IV. THE CONTACT PATCH REGION

There are two problems associated with attempting to define the region
or length of contact of the tire model pressed against a frictionless plane.
The first of these is the determination in some form or another of some of
the elastic constants which fit into the various equations of motion just
developed, particularly Eq. (22), which is the primary statement of deforma-
tion from the inflated state.

One method of accomplishing this is to observe that the static case
of Eq. (22), given in this report as Eq. (23), indicates that the static
problem of contact is a relatively simple one involving only a single
elastic constant, the dimensionless foundation modulus denoted here by the
symbol KA. It should be possible to determine the value of KA by appro-
priate tests on various real tires, in which certain deflections are im-
posed and the resulting contact patch lengths are measured. As a rough
estimate of the kinds of numbers to be obtained here, rather complete
tests have been run on two different pneumatic tires of 7.50x14.00 size,
one of these being a standard bias ply passenger car tire while the other
was a Michelin X-type passenger car tire of the same size. The detailed
results of these measurements will not be given in this report since they
will be presented as part of some forthcoming work in which methods of de-
termining the necessary constants for this tire model are discussed. How-
ever, it should be pointed out that in the usual region of deflection the

constant KA can be determined from a static test in which the length of

the contact patch of the tire is measured, and further, that rather major

differences appear between this constant as measured for the bias ply tire

and as measured for the X-type tire. For the particular tires mentioned,

the best average values of these constants worked out to be the following:

Bias Ply   350

X Type   190

This indicates that in general the constant KA may be determined from ex-

periment and used in subsequent calculations, such as in Eq. (22).

Similar techniques have not yet been developed for the direct measure-

ment of other elastic constants appearing in Eq. (22). For purposes of

this report, tire construction may be used as a guide in calculating some

of the constants appearing in this equation, and in this regard we are

rather fortunate in having the extensive background which exists in

material properties of cord rubber laminates. By the use of such informa-

tion one could generally hope to obtain the constants necessary in Eq. (22).

In connection with Eq. (22), one must next decide on techniques for

treating the deformation of the cylindrical shell model against a friction-

less plane. In doing this, it is seen that the left side of the equation

contains terms involving deflections while the right side contains only

the external pressure loading term. If one could know the deflections of

the shell model inside the contact patch region, then it might be possible

to specify the values z on the left side of Eq. (22) and to calculate the

particular values of θ for which the external pressure vanished, by means

of the right side vanishing in Eq. (22). This may be accomplished by

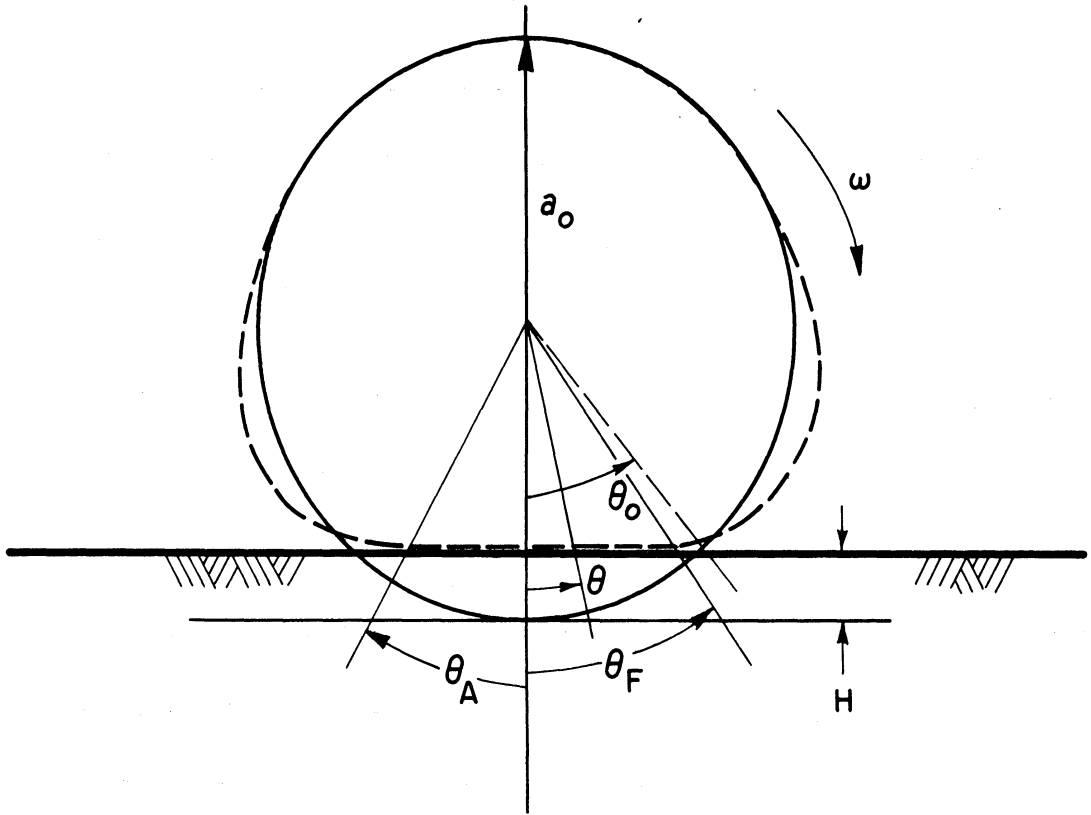reference to Figure 4 from which one may deduce by geometry that

Figure 4. Geometry of intersection of elastic shell with a rigid plane surface.

$$\bar{z} = -(1 - \frac{\cos\theta_0}{\cos\theta}) \tag{24}$$

where $\bar{z} = \frac{w}{a_0}$.

The first, second and fourth derivatives of this function are needed, and

these work out to be

$$\bar{z}' = \frac{\cos\theta_0}{\cos\theta} \left(\frac{\sin\theta}{\cos\theta} \right) \tag{25}$$

$$\bar{z}'' = \frac{\cos\theta_0}{\cos\theta} \left(\frac{1 + \sin^2\theta}{\cos^2\theta} \right) \tag{26}$$

$$\bar{z}^{IV} = \frac{\cos\theta_0}{\cos\theta} \left[\frac{5 + 18 \sin^2\theta + \sin^4\theta}{\cos^4\theta} \right] \tag{27}$$

16

Having these derivatives, it may be seen at once that given the proper elastic constants all terms of Eq. (22) may be evaluated by using Eqs. (24) - (27), which physically mean that the outer surface of the shell is in contact with the flat plane of Figure 4. We then search for the pressures PΘ in Eq. (22) which cause this situation to occur. Inside the region of the contact patch such pressures will be positive, while outside the contact patch region such pressures will be negative. Thus, we search for solutions to Eq. (22) in which the right hand side is zero. Such solutions must be functions of the angle Θ, and such solutions thus give angles Θ which define the ends of the contact patch.

Note that all functions on the left side of Eq. (22) are even except for the first derivative function which occurs in connection with the damping term. If the damping is nonzero, then it may be seen that the forward and aft angular locations of the contact patch will not be equal to one another, and in general this has been observed to be a fact. Use of Eq. (22) thus gives dynamic information concerning the contact patch in a rolling tire under the assumptions of complete contact with the flat plane.

In the later sections of this report several specific examples of the calculation of contact patch lengths under dynamic conditions will be presented. For the moment, the theory is complete and need only be worked out for the proper numerical cases.

V. FREE OSCILLATION OUTSIDE THE CONTACT PATCH REGION

For the region outside the contact patch, imagine the deflection z to be given by Eq. (19) of the previous chapter, noting that the contact pressure PΘ now vanishes. This causes the equation to become

$$z^{IV} + (2+WA)z'' - (CWA)z' + (1+KA-WA)z = PA+WA \qquad (28)$$

In Eq. (28) we are basically interested in two types of solutions, one forward of the contact patch leading edge and the other aft of its trailing edge. Accordingly, the solutions will be split into the two parts and considered separately.

Considering first the region forward of the leading edge of the contact patch, one has in accordance with Figure 4 all values

$$\Theta > 0$$

In this region we will consider particular solutions to Eq. (28) as well as the solution to its complementary form. Thus, the total displacement z will be of the form

$$z = z_c + z_p \qquad (29)$$

where the particular solution is given by

$$z_p = \frac{PA+WA}{1+KA-WA} \qquad (30)$$

The complementary solution of Eq. (28) will be in the general form

$$z_c = Ae^{q\Theta_1} \qquad (31)$$

which, upon substitution into the complementary form of Eq. (28) gives

$$q^4+(2+WA)q^2-(CWA)q+(1+KA-WA) = 0 \tag{32}$$

We must now search for the four roots q, which in general will be complex numbers. In view of the large number of different possible combinations of parameters which are to be considered, it is perhaps best to approach Eq. (32) numerically. This may be accomplished by setting

$$q = d+ib$$

which, upon substitution into Eq. (32), yields

$$(d^2-b^2)^2-4d^2b^2+4db(d^2-b^2)i+(2+WA)[(d^2-b^2)+2dbi] \tag{33}$$

$$-(CWA)(d+ib) + (1+KA-WA) = 0$$

Equation (33) may be separated into its real and imaginary parts. This gives two distinct equations, each of which must vanish. These are of the form

$$(d^2-b^2)^2-4d^2b^2+(2+WA)(d^2-b^2)-(CWA)d+(1+KA-WA) = 0 \tag{34}$$

$$4db(d^2-b^2)+(2+WA)2db-b(CWA) = 0 \tag{35}$$

From Eq. (35), one may solve

$$d^2-b^2 = \frac{CWA}{4d} - \frac{(2+WA)}{2} \tag{36}$$

Substituting this into Eq. (34) gives

$$\left[\frac{CWA}{4d} - \frac{(2+WA)}{2}\right]^2 - 4d^2\left[d^2- \frac{CWA}{4d} + \frac{(2+WA)}{2}\right]$$

$$+ (2+WA)\left[\frac{CWA}{4d} - \frac{(2+WA)}{2}\right] - (CWA)d +(1+KA-WA) = 0 \tag{37}$$

Multiplying Eq. (37) by d^2, and collecting coefficients of d, one obtains an equation involving only the real part, d, of the complex number q.

$$-4d^6 - 2d^4(2+WA) + d^2[-\frac{(2+WA)^2}{4} + (1 + KA - WA)]$$

$$+ (\frac{CWA}{4})^2 = 0 \tag{38}$$

Examination of the coefficients of Eq. (38) shows that it will yield three distinct values for d^2. Of these, one will be negative, one positive and one complex. Returning to the original assumption for the nature of d, it is seen that it is by definition a real number so that only the positive root of Eq. (38) is of interest here. The others may be neglected as physically meaningless in this situation. From the positive root for d^2 from Eq. (38), one will obtain equal positive and negative values of the constant d in this problem.

From Eq. (36), one may solve for the constant b associated with each particular d in the form

$$b^2 = d^2 - \frac{CWA}{4d} + \frac{(2+WA)}{2} \tag{39}$$

It may be seen from this equation that there will be a value of b associated with each value of d. If one uses the positive value of d in the Eq. (39), then a corresponding value of b will be obtained, while if one uses a negative value of d, a different value of b will result. Accordingly, a notation will be adopted to handle this as shown in Eq. (40). It should be emphasized that the numerical values of b_F and b_A are different.

$$+d \rightarrow b_A \qquad -d \rightarrow b_F \tag{40}$$

Using the values of d and b obtained from Eqs. (38) and (39) respectively, one may return to the original form of the solution to this equation, given as Eq. (31), and note that the result of having available these four

combinations of d and b values allows the final solution to the complementary form of Eq. (28) to be written as

$$z_{CF} = e^{d\Theta_1} (A \sinb_A \Theta_1 + B \cos b_A \Theta_1)$$
$$+ e^{-d\Theta_1} (C \sinb_F \Theta_1 + D \cos b_F \Theta_1) \tag{41a}$$

In using Eq. (41), one must keep in mind that the complete solution for deflection is given by Eq. (29), in which the particular solution is added to the one just obtained.

In this particular case it appears easiest to utilize the solution as given by Eq. (41) by means of shifting the Θ_1 origin to the forward edge of the contact patch. This has no numerical effect on the solutions to the motion in the free region, but does make it possible to satisfy the boundary conditions in a somewhat easier way algebraically. Before proceeding to that, it is desirable to note that Eq. (41) contains two different types of terms, one involving positive exponentials and the other negative exponentials. In view of the fact that the constant d is expected to be of some reasonable size, and in view of the fact that the boundary conditions at the top of the rolling wheel (defined by $\Theta = \pi$), would require very small values for the constants A and B, it is felt that one may approximate the solution to this problem by considering that the only portions of this solution which are valid and operative near the forward edge of the contact patch are those portions associated with the negative exponentials. This, in effect, assumes that the cylinder is of indefinite diameter compared to the size of the contact patch. It is an approximation which turns out to

21

be reasonably well justified by subsequent calculations. Hence, one may write for the region forward of the contact patch

$$z_{CF} = e^{-d\Theta_1}(C \sin b_F \Theta_1 + D \cos b_F \Theta_1) \qquad (41b)$$

We will subsequently provide initial conditions for determining the constants of integration C and D of Eq. (41), by means of matching the deflection and slope of the free shell at the leading edge of the contact patch with the corresponding deflection and slope of the constrained shell at this same point.

For the portion of the shell aft of the trailing edge of the contact patch, one will have a very similar solution to that just obtained for the forward portion. Such a solution may generally be set down, using primes to denote it from the previous one, in exactly the same form as is done in Eq. (42)

$$z_{CA} = e^{d\Theta_1}(A' \sin b_A \Theta_1 + B' \cos b_A \Theta_1)$$
$$+ e^{-d\Theta_1}(C' \sin b_F \Theta_1 + D' \cos b_F \Theta_1) \qquad (42)$$

Here, we wish to set a new origin at $\Theta = -\Theta_{aft}$, and to direct the positive Θ direction in this case to the rear. Hence, we set

$$\Theta_1 = -\Theta_1'$$

This causes Eq. (42) to take on the form

$$z_{CA} = e^{-d\Theta_1}(-A' \sin b_A \Theta_1' + B' \cos b_A \Theta_1')$$
$$+ e^{d\Theta_1}(-C' \sin b_F \Theta_1' + D' \cos b_F \Theta_1') \qquad (43)$$

Disregarding the positive exponential portion of this gives an approxima-

tion to the solution of the form

$$z_{CA} = e^{-d\Theta_1'}(-A'\sin b_A\Theta_1 + B'\cos b_A\Theta_1) \tag{44}$$

Again, the complete solution for the aft portion of the wheel outside the contact region is given by

$$z_A = z_{CA} + z_p$$

We now have complete solutions for motion both forward and aft of the contact patch in the region not in contact with the plane of rolling. It is next necessary to set up conditions by means of which the constants of integration of Eqs. (41) and (44) may be obtained. It would be desirable to have four constants of integration associated with each of the solutions given by Eqs. (41) and (44). This would be necessary if one wished to match deflection, slope, bending moment and shear force in the free shell region with those quantities at the end of the contact patch region. Having only two constants of integration available for each solution, it is only possible to match the quantities of primary importance, namely the deflection and slope. Accordingly, the matching equations are

$$z_F(o) = \bar{z}(\Theta_F) \tag{45a}$$

$$\left(\frac{dz_F}{d\Theta_1}\right)_{\Theta_1=o} = \bar{z}_F'(\Theta_F) \tag{45b}$$

$$z_A(o) = z(-\Theta_A) \tag{45c}$$

$$\left(\frac{dz_A}{d\Theta_1'}\right)_{\Theta_1=o} = -\bar{z}'(-\Theta_A)$$

where the contact patch area deflection is given by Eq. (24) and the contact patch slope is given by Eq. (25).

Using Eqs. (24) and (25), along with Eqs. (45), the constants of integration in Eqs. (41) and (44) may be obtained in the form

$$D = \left(\frac{\cos\Theta_O}{\cos\Theta_F} - 1\right) - \left(\frac{PA+WA}{1+KA-WA}\right) \tag{46a}$$

$$C = \left(\frac{d}{b_F}\right)D + \frac{1}{b_F}\left(\frac{\sin\Theta_F\cos\Theta_O}{\cos^2\Theta_F}\right) \tag{46b}$$

$$B' = \left(\frac{\cos\Theta_O}{\cos\Theta_A} - 1\right) - \left(\frac{PA+WA}{1+KA-WA}\right) \tag{46c}$$

$$-A' = \left(\frac{d}{b_A}\right)B' + \frac{1}{b_A}\left(\frac{\sin\Theta_A\cos\Theta_O}{\cos^2\Theta_A}\right) \tag{46d}$$

Use of these constants of integration still leaves the second and third derivatives of dimensionless displacement z discontinuous at the junction of the contact patch and free tire region. The bending moment mismatch has been investigated numerically and generally is small. It is based upon the definition of moment obtained from Ref. 4, and given in Eq. (47).

$$M_\phi = \frac{Eh^3}{12a^2} \cdot b_W \cdot (w+w'') \tag{47}$$

where a is the radius of the cylindrical shell once again. Using the moment equilibrium of a small element of shell, the shear force becomes

$$Q = \frac{Eh^3}{12a^2} b_W(z'+z''') \tag{48}$$

The first derivative z' in Eq. (48) is matched at the interface or junction between the region in contact and the free region of the shell. Hence the total concentrated shear force necessary there, represented by the shear mismatch, is given by

$$Q_F = \frac{Eh^3}{12a^2} b_W[z_F'''(o)-\bar{z}'''(\Theta_F)] \tag{49a}$$

$$Q_A = \frac{Eh^3}{12a^2} \cdot b_W \cdot [z_A'''(o) - \bar{z}'''(\Theta_A)] \qquad (49b)$$

Now from the expressions previously developed, namely Eqs. (41) and (44), one may write a third derivative as

$$z_F''' = e^{-d\Theta_1}\left[C\left\{[b_F(d^2-b_F^2)+2db_F^2]\cos b_F\Theta_1 \right.\right.$$

$$+[2db_F^2-d(d^2-b_F^2)]\sin b_F\Theta_1\Big\} + D\Big\{[2db_F^2-d(d^2-b_F^2)]\cos b_F\Theta_1 \qquad (50)$$

$$\left.\left.+[-2d^2b_F-b_F(d^2-b_F^2)]\sin b_F\Theta_1\right\}\right]$$

and

$$z_A''' = e^{-d\Theta_1}\left[-A'\left\{[b_A(d^2-b_A^2)+2db_A^2]\cos b_A\Theta_1 \right.\right.$$

$$+[2db_A^2-d(d^2-b_A^2)]\sin b_A\Theta_1\Big\} + B'\Big\{[2db_A^2-d(d^2-b_A^2)]\cos b_A\Theta_1 \qquad (51)$$

$$\left.\left.+ [-2db_A^2-b_A(d^2-b_A^2)]\sin b_A\Theta_1\right\}\right]$$

from which the shear forces at the forward edge of the contact patch and at the aft edge of the contact patch become respectively,

$$Q_F = \frac{b_W Eh^3}{12a^2} [z_F'''(o) - \bar{z}'''(\Theta_F)] \qquad (52a)$$

$$Q_A = \frac{b_W Eh^3}{12a^2} [z_A'''(o) + \bar{z}'''(-\Theta_A)] \qquad (52b)$$

The vertical load carried by the tire, as well as the drag force caused by shifting of the center of pressure from directly under the axle point, may be calculated now if one knows the angles Θ_F and Θ_A, defining the contact patch position. Letting P represent total vertical load and MO moment of this load about the axle, one obtains

$$P = p_0 \cdot a \cdot b_W(\Theta_F+\Theta_A) + Q_F + Q_A \qquad (53)$$

25

$$MO = p_o \frac{a^2 bw}{2} (\Theta_F^2 - \Theta_A^2) + a' Q_F b_F \qquad (53)$$

$$- a^* Q_A {}^\bullet \Theta_A$$

A real question arises concerning the existance of such concentrated

shear forces as given by Eqs. (52). In a real tire, in which a soft outer

tread is used as a scuff resistant cover, there is some doubt whether such

concentrated forces could be generated by means of a mismatching of the third

derivatives of displacement. What more probably happens is that this soft

outer cover actually forces the displacement and its derivatives to be con-

tinuous at the junction of the contact patch with the free portions of the

shell, so that in many cases, in fact most all cases, such concentrated

forces cannot exist. This seems to be partially confirmed by static pressure

distribution tests down the length of a contact patch, which show consider-

able similarity to calculations which are done on the basis of no concen-

trated forces. These are presented later on in the succeeding chapters of

this report. The measurements cited, however, are static measurements and

no similar measurements apparently exist for relatively high speed rolling

conditions. It may be surmised that for relatively high speed conditions

one would find it harder and harder to consider that the tread actually pre-

vents the mismatch of the shear forces as given by Eqs. (52). In this case,

one might visualize that some influence of such shear forces would indeed

appear at higher speeds. At the present time we are not in a position to

answer this speculation in any quantitative way, since it would require

either the addition of shear deformation to the present theory or a modifi-

cation of the present theory to include a relatively soft tread around the running band. Both of these approaches have been investigated briefly and seem to lead into formulations of considerable complexity. While it is not implied that such theories would be impossible to carry out, it is felt that their utility might be somewhat restricted by their length and the difficulty of solution of the equations which they generate. For that reason, we will attempt here to construct this theory primarily on the basis of the fact that these concentrated forces clearly do not appear during static measurements, and hence it will be assumed that they do not appear at all during the rolling process. It should be understood that this assumption may be subject to a revision as more information becomes available and as more familiarity with these equations is obtained.

VI. TYPICAL EXAMPLES AND CALCULATIONS

There are at least two methods for attempting to verify some of the theoretical ideas brought out by the use of a model such as proposed in this report. Perhaps the best and most direct of these would be to manufacture a model of the type visualized here and to actually conduct tests involving its rolling over some essentially frictionless plane, in such a way that pressure distributions, total vertical loads and drag forces could be measured accurately. If the properties of the model were well known, then the predictions of the theory could be compared with measured data. A certain amount of this type of testing and comparison has been done in connection with various point load problems, which are not discussed in this report. However, such a series of experiments becomes rather difficult when they must be done on a flat plane as visualized here, since the equipment for rolling a wheel on such a flat surface is expensive and complicated. For that reason a different approach will be used in this report, where we will attempt to utilize characteristics which closely approximate those of a real tire, and attempt to predict some of the known operating characteristics of such a tire. In some respects this is less satisfactory than the first process, since it is known that many of the important operating characteristics of a tire depend heavily on its internal loss characteristics. These internal loss characteristics are not yet well known for rubber-cord combinations. It is clear that a simple viscous loss law does not represent

such loss characteristics very well, and so in our calculations it will not be possible to exactly represent the behavior of any real tire in operation. For this reason it should be pointed out clearly that the purpose of this report is not to model a specific tire exactly, but rather to introduce a technique which, given the proper loss characteristics, can be used to perform such modeling. Hence, in the subsequent calculations rather idealized loss laws are used simply because their form is readily available. The resulting calculations are indications of the general nature of tire behavior under such conditions. The fact that some of their important characteristics seem to agree with actual tire characteristics gives hope that the theoretical framework outlined here will have some utility as a tool in predicting the overall operating characteristics of a real pneumatic tire.

One must first turn to the constants needed in evaluating the various equations in this report. Basically, these constants are exactly those which one must use to define the overall characteristics of a circular cylindrical shell of the type proposed here. An attempt has been made to chose such characteristics to be compatible with a 7.50x14.00 automotive tire, and the resulting numerical values are being used for subsequent calculations.

$$b_w = 4.625 \text{ in.} \qquad\qquad E = 2500 \text{ psi}$$

$$a = 12.35 \text{ in.} \qquad\qquad h = 1.50 \text{ in.} \qquad (53)$$

$$a_o = 13.35 \text{ in.} \qquad\qquad \rho = 1 \times 10^{-4} \text{ lb-sec}^2/\text{in.}^4$$

Using this particular value of the outside radius of the wheel a_o, namely

13.35 in., one finds that the angular velocity is related to the linear

speed in miles per hour by the relation

$$\Omega = 1.32 \text{ rad/sec/mph.} \tag{54}$$

Consider next the problem of calculating the response of a pneumatic

tire having the properties given in Eqs. (53) under conditions of given

velocity and load. For this purpose, one must first specify the loss law

to be used. As a first example, the viscous loss type of law discussed in

the main body of this report will be utilized, and we will choose a value

of the damping factor c to be

$$c = 0.13 \tag{55}$$

This is based on interpretation of oscillograph records from free vibration

tests of a pneumatic subjected to an impulsive blow. A digital computer

program has been constructed which first calculates the forward and aft

edges of the contact patch at a fixed value of damping constant, and for

various values of the other parameters listed in Eqs. (53) and (54). This

is done by specifying the tire deflection, which is effectively accomplished

by fixing the angle Θ_o of Eq. (24) or of Figure 4. Next, for the viscous

loss law, the motion of the shell in the free region forward and aft of the

contact patch is calculated by means of Eqs. (38) and (39). Eq. (38) gives

the damping factor while Eq. (39) or (40) gives the forward and aft wave

numbers b. These quantities define the motion of the free region, and are

readily calculated from the expressions developed. For this particular ex-

ample, the deflection Θ_o will be caused to vary between 0.3 and 0.5, while

30

the linear velocity will be allowed to range from 0 to 120 miles per hour

and the inflation pressure will take on two values, namely 24 psi and 40

psi.

As a check, it should be noted that in general drag losses are larger

for the larger inflation pressure, a condition which is verified by experi-

ment.

In these calculations, it is necessary to have some value for the

dimensionless foundation modulus $\bar{k}/\alpha^2 = KA$, which has been previously dis-

cussed. It was pointed out in Rept. 18 of this series that this quantity

can be obtained directly from a static test in which the length of the con-

tact patch is measured. In doing this on two real tires, a conventional

bias ply tire and a Michelin belted tire gave values of 350 and 190 for

this constant, respectively. Hence, the calculations will also be allowed

to range over both of these specific values as a means of generally com-

paring the operating conditions of a bias ply tire of those with a belted

tire.

The results of these calculations are first given in Figure 5. Here,

the forward and aft boundaries of a typical contact patch are plotted as a

function of rolling velocity for two different inflation pressures and two

different values of the dimensionless foundation modulus KA, corresponding

to the bias ply and belted tires. It may be seen that for the bias ply tire

the static value of the contact patch length is considerably longer than for

the radial tire, but at about 40 miles an hour the radial tire exhibits a

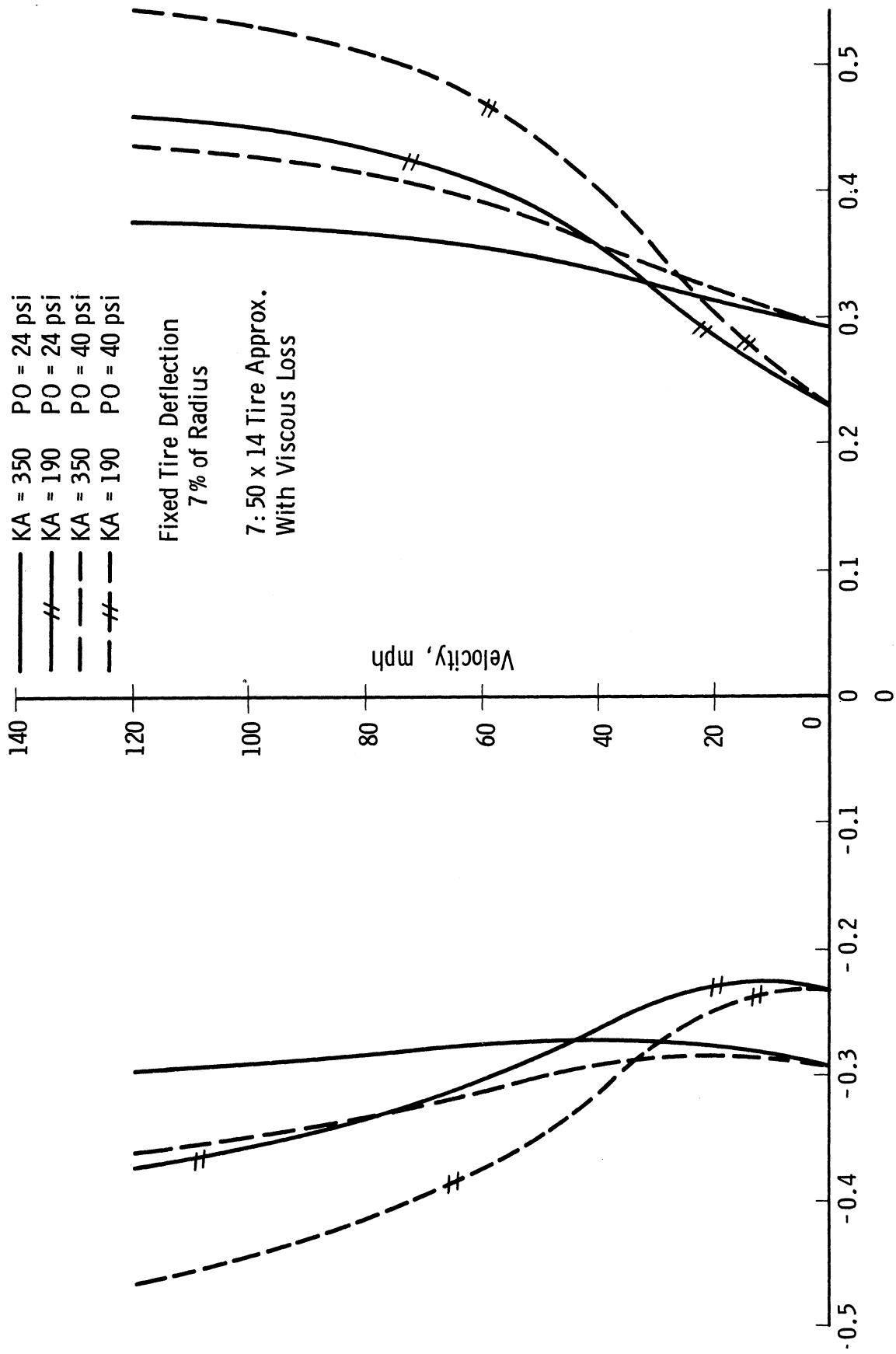growth of the contact patch which makes the two equal at that speed, and at

Figure 5. Contact patch position vs. velocity.

Legend (within figure):

KA = 350   PO = 24 psi
KA = 190   PO = 24 psi
KA = 350   PO = 40 psi
KA = 190   PO = 40 psi

Fixed Tire Deflection
7% of Radius

7:50 x 14 Tire Approx.
With Viscous Loss

Velocity, mph

32

all higher velocities the radial tire exhibits a greater length of contact patch for the fixed tire deflection.

In Figure 5, the angle θ_0 was set to be 0.375.

One might deduce from Figure 5 that the rolling radius of a belted tire would tend to increase more rapidly with speed than the rolling radius of a bias ply tire. One might also note that generally speaking the bias ply tire exhibits a forward shift of the contact patch with speed, in that the forward and aft edges both move forward with velocity. This causes the entire pressure distribution to move forward and results in a shift of the center of pressure forward of the axle point so as to cause a drag force. In the case of the belted tire, as defined by the constant KA = 190, the growth of the contact patch occurs in both fore and aft directions, but it is greater in the forward direction than in the aft direction.

It may be seen that the influence of inflation pressure is to cause the contact patch lengths to be longer as the inflation pressure is increased.

In Figure 6 are shown curves of the influence of rolling velocity on vertical load carried at constant tire deflection. These curves are plotted for two different values of inflation pressure and for values of the parameter KA corresponding to the bias ply and belted tire. For the lower pressure of 24 psi, it may be seen that at constant deflection the belted tire carries a smaller load than the bias ply, but that this situation reverses at a rolling velocity of about 40 miles per hour, where the belted tire begins to pick up more vertical load than the bias ply tire.
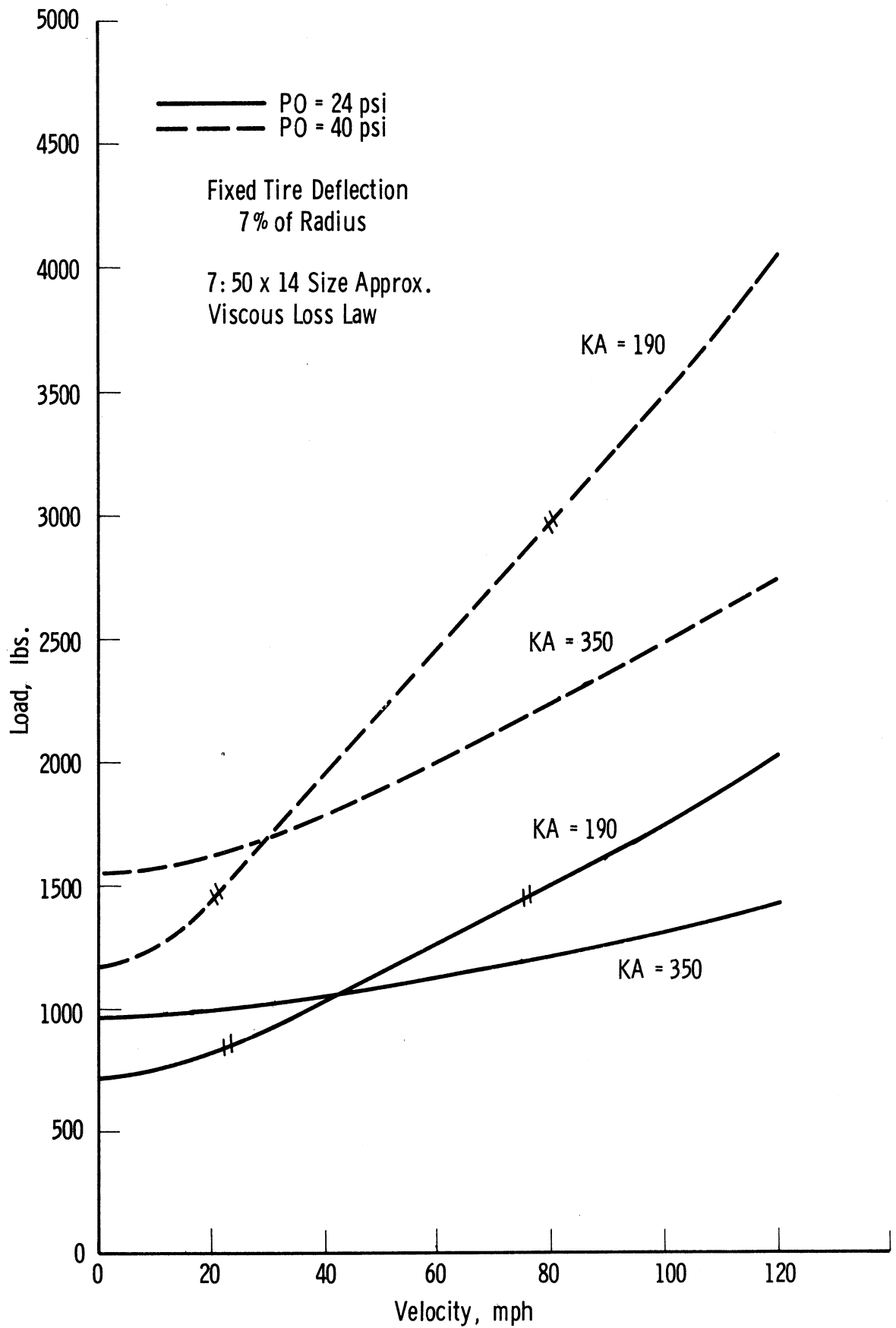
33

Figure 6. Vertical load vs. velocity.

A similar situation exists at a higher inflation pressure of 40 psi, where the crossover point between equality of load carrying capacity occurs at about 30 miles per hour. In this case, the belted tire picks up large loads at high velocities and it is clear from such a diagram as Figure 6 that at constant load the rolling radius of a belted tire would increase considerably with speed at higher inflation pressures.

In Figure 7, the drag force is plotted as a function of rolling velocity for the same parameters as covered in Figure 6, namely two values of internal pressure and two values of foundation modulus KA corresponding to belted and bias ply tires. It should be emphasized that these curves are almost entirely dependent upon the detailed form of the loss law which was assumed in making the calculations. As will be recalled, this loss law was taken to be a simple viscous function, which is known to be inaccurate, but was chosen merely for simplicity. Using this function, one may refer to Figure 7 and note that generally drag forces, expressed as pounds of force at the axle, increase with velocity. The drag forces at higher inflation pressures are greater for constant deflection than the drag forces for lower inflation pressures. This is in general in accordance with observations. However, in all cases the drag forces associated with the belted tire appear to be greater than the drag forces associated with a bias ply tire. Since both the belted and bias ply tire calculations were performed using the same value of the viscous loss coefficient, this might indicate that the reduced rolling resistance reported in belted tires arises due to inherently lower internal hysteresis characteristics rather than to dynamic effects.
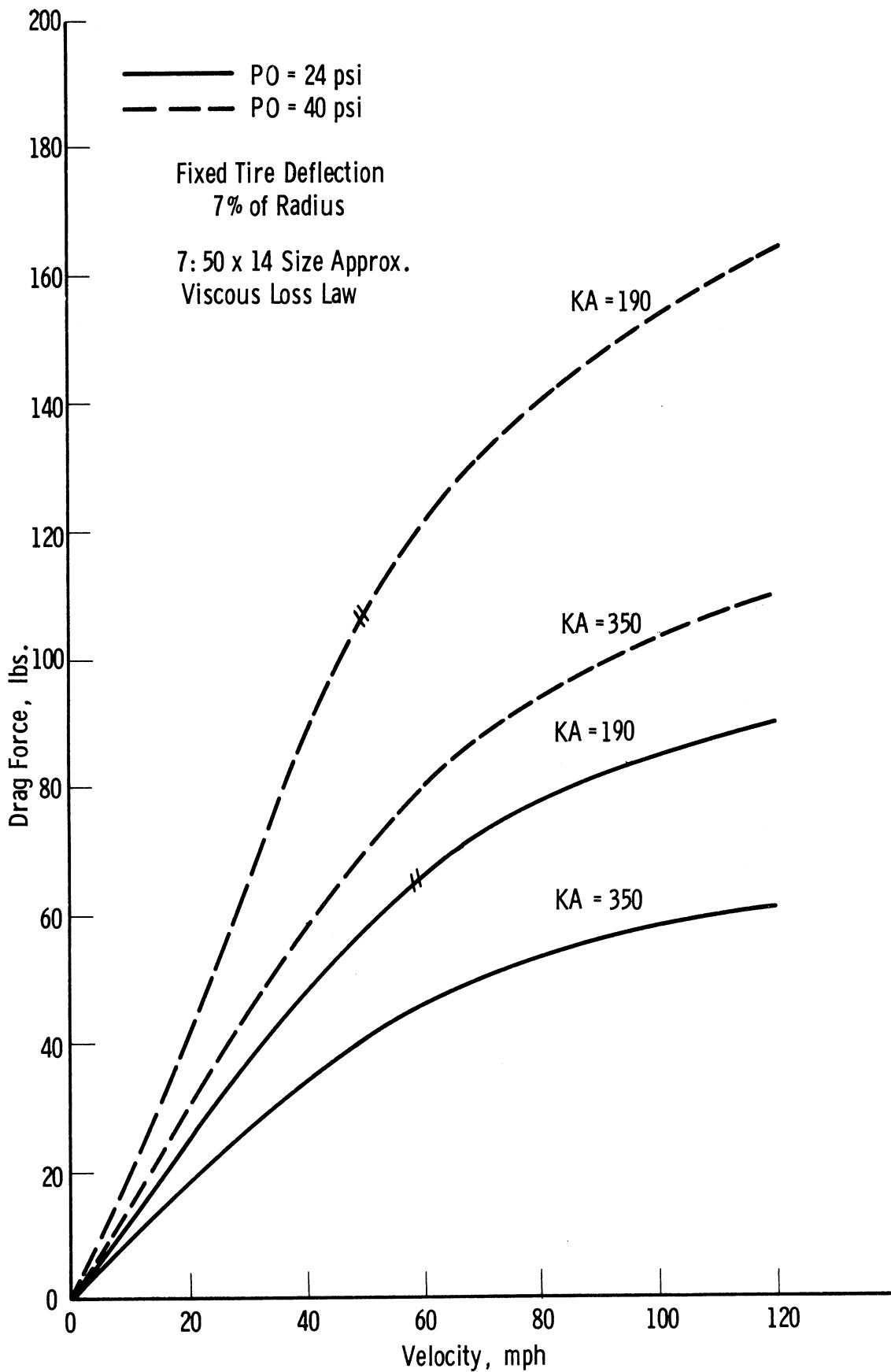
Figure 7. Drag force vs. velocity.

36

Subsequent calculations contradict this, however. It should also be noted that Figure 7 does not contain any loss from the scrubbing in the contact patch, and this may also be a factor in comparing bias ply and belted tires. Figure 7 is intended as a general presentation of the type of information which can be obtained by calculation from this model, and should not be construed as representing the specific characteristics of the model.

In Figure 8, the maximum contact pressures in the contact patch are plotted as a function of rolling velocity for the same four cases as treated previously, the two internal pressures and the two values of the foundation modulus. The general results obtained from this set of calculations seem to indicate that at low rolling velocities the bias ply tire exhibits a higher contact pressure with the ground while at somewhere between forty and sixty miles per hour the belted tire begins to show higher pressures so that at extremely high speeds the maximum contact pressures with the tire of lower foundation modulus are markedly greater.

The results shown in Figure 8 seem to indicate that at the usual inflation of 24 psi, contact pressures would normally not exceed 40 psi under ordinary driving conditions.

Figure 9 shows plots of the contact pressure distribution in the contact patch at two different speeds, at 0 and 100 miles per hour, and for the two values of the foundation modulus previously discussed. Here, it may be seen that under static conditions the bias ply tire exhibits a longer contact patch with higher pressures than does the belted tire. Hence, under static conditions of equal deflection the bias ply tire will carry considerably
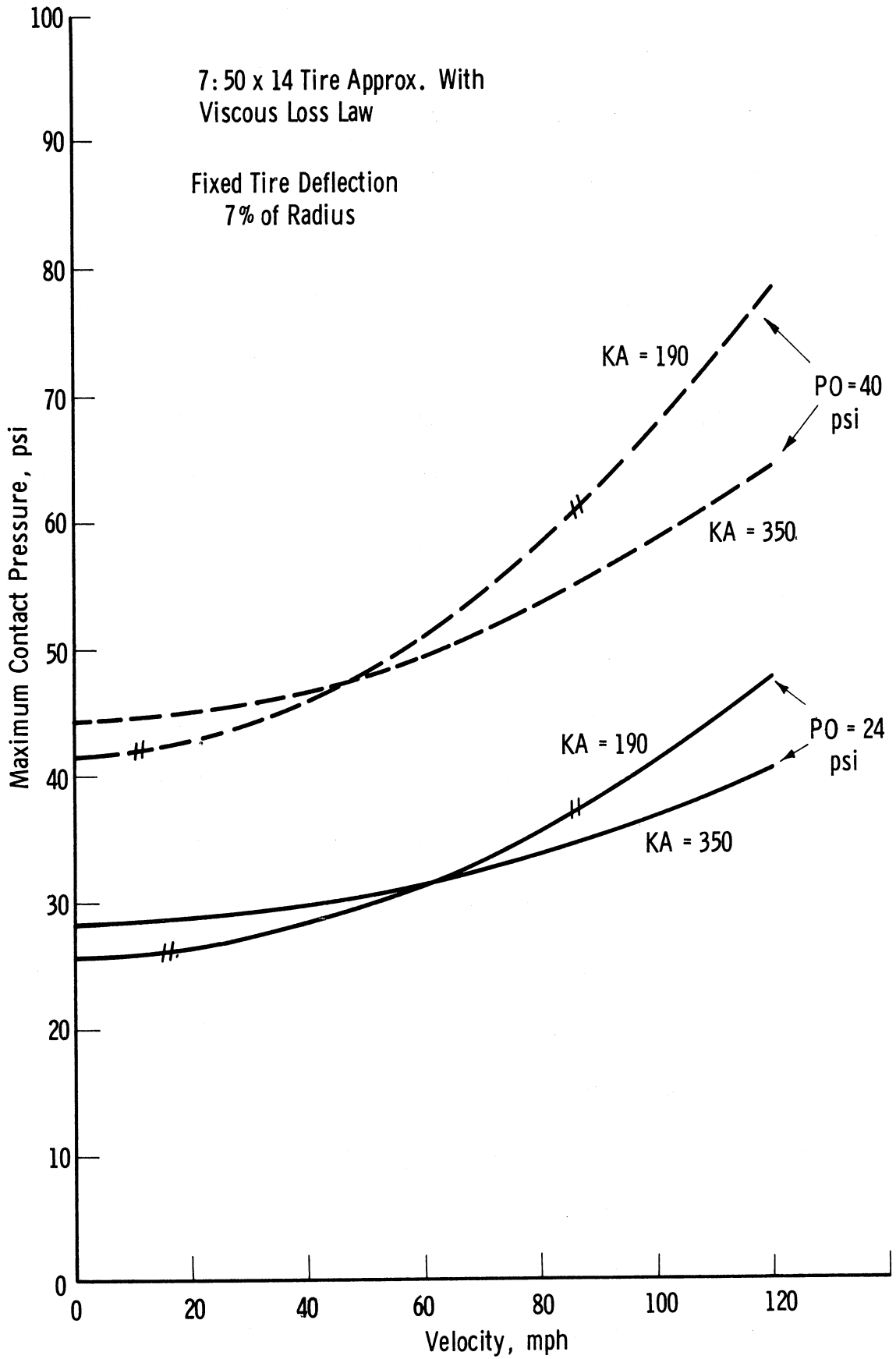
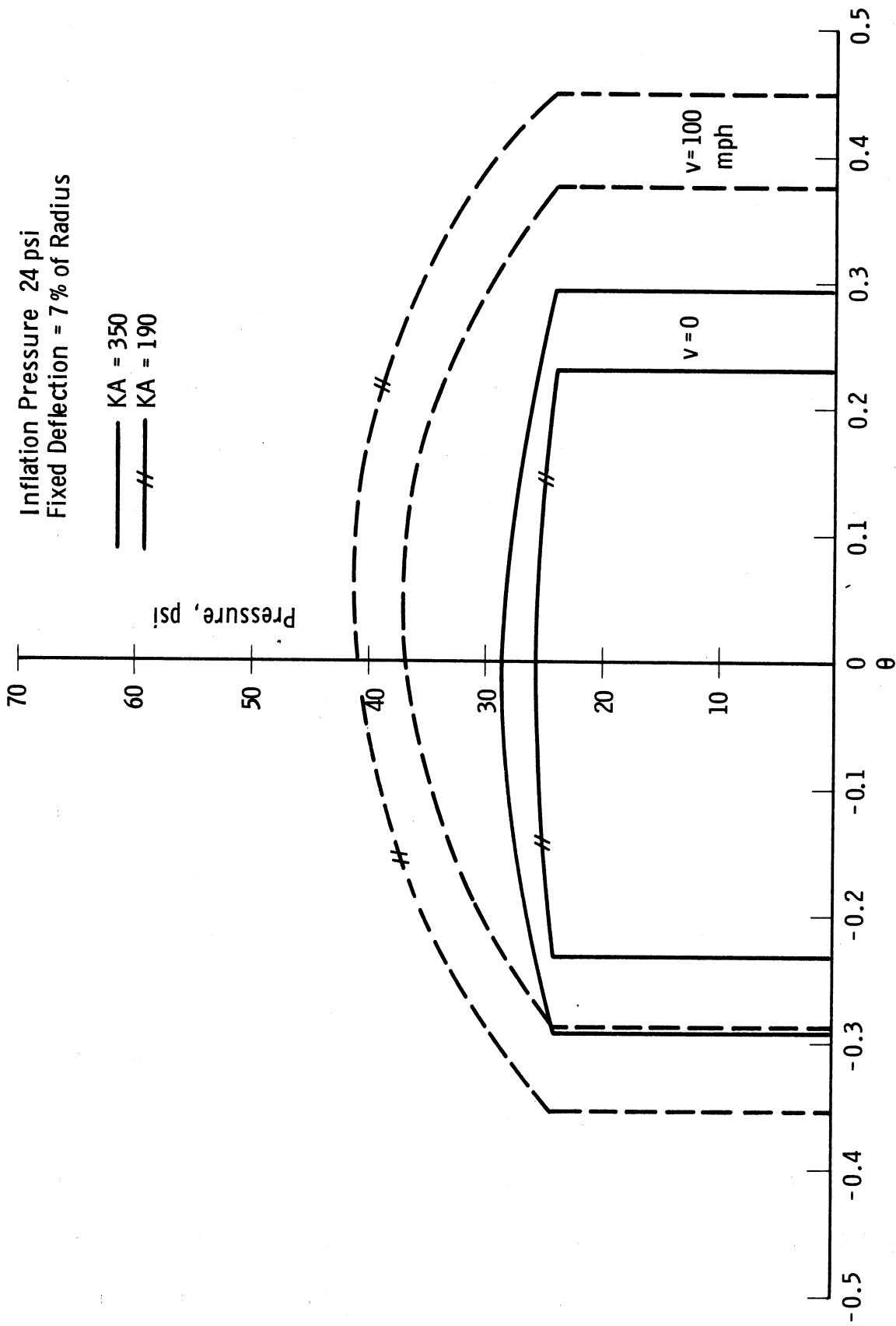Figure 8. Maximum contact pressure vs. velocity.

Figure 9. Contact pressure vs. position for static and 100 mph conditions.

39

more load, as is shown in the calculations and in the curves of Figure 6. On the other hand, at a rolling velocity of 100 miles per hour the situation has reversed and the bias ply tire now exhibits a smaller contact length along with lower contact pressures, thus allowing the belted tire to carry considerably greater load.

The static pressure distributions are symmetric and come close to being rectangles. On the other hand, the dynamic pressure distributions evaluated at 100 miles per hour show rather large differences between the peak pressure near the center of the contact patch and the inflation pressure. In addition, the entire pressure distribution has shifted forward. This causes a forward movement of the center of pressure which results in drag forces.

In Figure 10, plots are given of three of the parameters describing the wave shape outside the contact patch region as a function of the rolling velocity. The damping factor d is plotted as a function of velocity, and it may be seen that it drops very abruptly from a relatively high value of 20 miles per hour to a small value at 100 miles per hour. This is also in accord with general observations that the damping must decrease as speed increases.

The wave number pertaining to shell displacement aft of the contact patch is also plotted in Figure 10, and first increases and then decreases. This indicates that the wave length of bending displacement behind the contact patch reaches a minimum at about 40 miles per hour and then continues to increase as the speed increases from there on. The forward wave number is also plotted in Figure 10 and it may be seen that this increases rapidly
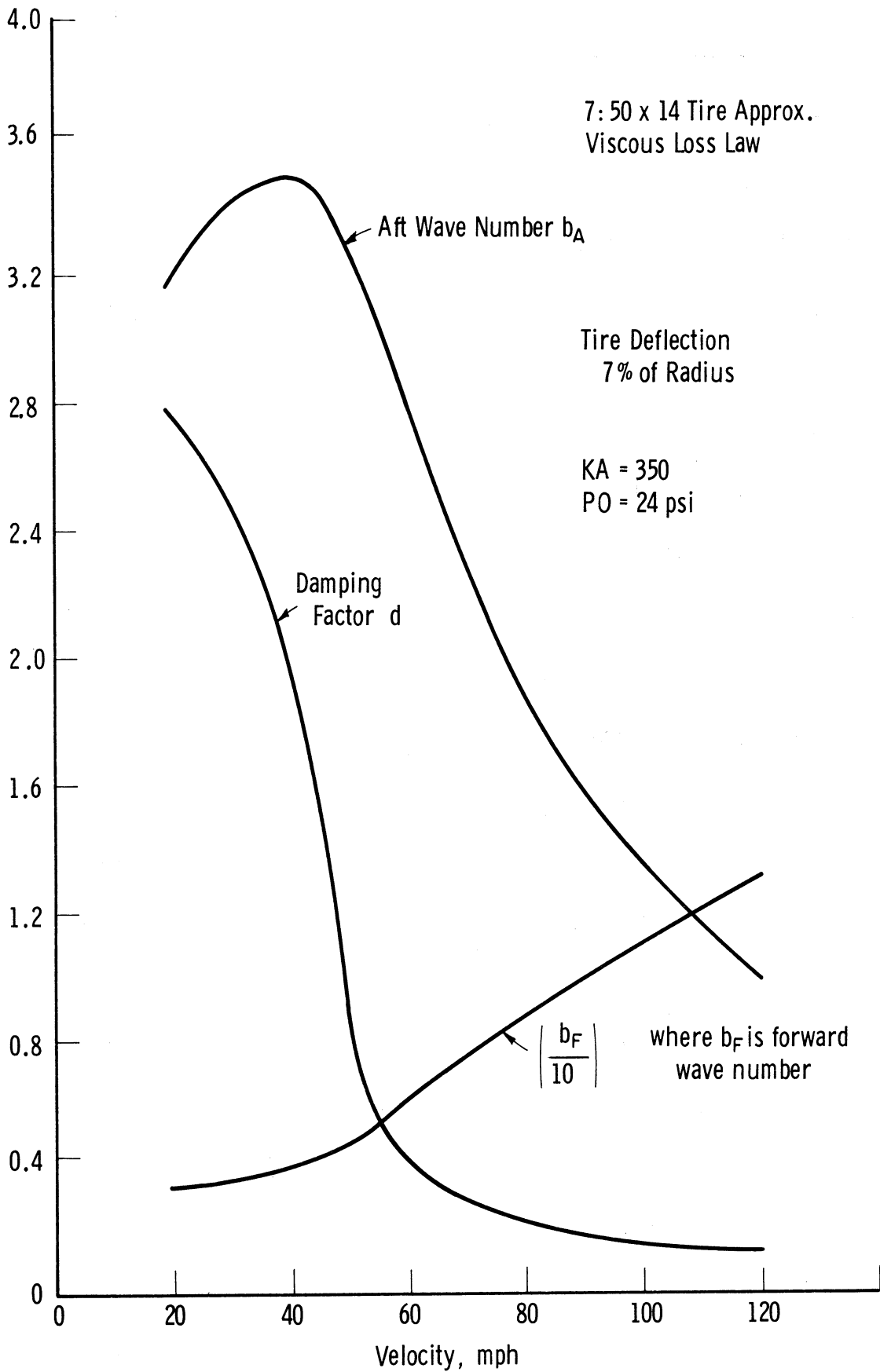
40

Figure 10. Typical values of damping factor and wave number vs. velocity.

with velocity, as can be observed by noting that it is necessary to plot

this wave number to one tenth scale in order to accomodate it to the scale

of Figure 10. The fact that this wave number rises so rapidly indicates

that very high frequency waves are being generated just forward of the con-

tact patch, and these, of course, will give rise to relatively severe bend-

ing stresses due to their high frequency nature. This also is in general

accord with observations of the critical speed phenomena.

In general it might be said that by use of the equations discussed in

the preceeding sections it is possible to calculate most of the important

quantities dealing with the rolling of a pneumatic tire in a straight line

under constant velocity conditions. One very important characteristic in

such calculations is the form of the loss laws, since this determines al-

most completely the general form of the drag forces which are generated

and also dictates to some extent the nature of the contact patch shift as

velocity increases. Therefore, it should be emphasized that users of this

type of mathematical model will probably find it necessary to generate

their own individual loss laws and to insert them into the appropriate

equations of this report. Only by this process will it be possible to ob-

tain realistic tire performance data from a mathematical model such as

this. An example of this type of loss law is given in the subsequent

numerical example.

It should be noted in closing this discussion of the viscous loss law

that examination of the equations concerning the forward and aft wave num-

bers and the damping constant d will indicate at once that these are in-

dependent of the deflection imposed on a tire. This means that the wave

phenomena can be generated by small as well as large deflections, and hence

that the critical speed, if one exists, is quite independent of the load

carried on the tire or its deflection.

VII. STRUCTURAL DAMPING

An alternate approach to the use of viscous damping is to attempt

to write some simple expression involving structural damping as a mechanism

of loss in a pneumatic tire model. In order to do this, we may draw upon

various simple descriptions of structural damping, such as that of Tong[6].

There, structural damping is defined as damping which is proportional in

magnitude to the elastic forces and is directed opposite to the velocity.

In this case, we choose to define the elastic forces as the elastic forces

in the foundation of the circular shell. According to the definition of

structural damping, a radial pressure is generated, due to such damping,

of magnitude given by Eq. (56)

$$p_r = \left| \frac{gkw}{\dot{w}} \right| \dot{w} \tag{56}$$

Note that this may be treated within the framework of the same general

equations previously written by inserting this radial pressure in place of

the one previously defined for viscous forces, and that such a substitution

will give an equation of the motion of the form

$$\alpha^2(w^{IV} + 2w'' + w) + \frac{a^2}{Eh} \rho h(\ddot{w} - \Omega^2 w) + \frac{a^2}{Eh}\left(kw + \left| \frac{gkw}{\dot{w}} \right| \dot{w}\right)$$

$$\frac{a^2}{c_1^2}\ddot{w} + \frac{a^2}{Eh} gk\dot{w} \; Q + \alpha^2 w^{IV} + 2\alpha^2 w'' \tag{57}$$

$$+ w\left[\alpha^2 + \frac{ka^2}{Eh} - \frac{\Omega^2 a^2}{c_1^2}\right] = \frac{a^2}{Eh}[p_o - p(\Theta) + \rho h a \Omega^2]$$

where
$$Q = \left| \frac{w}{\overset{*}{w}} \right|.$$

This may be compared with Eq. (9). It is now necessary to transform this equation into moving coordinates, as previously described. This results in the expression for steady state motion given by Eq. (58).

$$z^{IV} + (2 + \frac{\overline{\Omega}^2}{\alpha^2})z'' - g\frac{\overline{k}}{\alpha^2} \left| \frac{z}{\Omega z'} \right| \Omega z' + (1 + \frac{\overline{k}}{\alpha^2} - \frac{\overline{\Omega}^2}{\alpha^2})z$$

$$= -\frac{p}{\alpha^2} + \frac{\Omega^2}{\alpha^2} + \frac{p_0}{\alpha^2} \tag{58}$$

This may be compared with Eq. (17). In Eq. (58), the radial pressure due to the structural damping has been transformed into

$$p_r = -gk \left| \frac{w}{\overset{*}{w}-\Omega w'} \right| (\overset{*}{w}-\Omega w') \tag{59}$$

from which the steady state conditions give rise to the radial pressure

$$p_r = gk\Omega z' \left| \frac{z}{\Omega z'} \right| \tag{60}$$

The dimensionless version of this equation of motion then reduces to

$$z^{IV} + (2+WA)z'' - gz'\Omega(KA) \left| \frac{z}{\Omega z'} \right| +$$

$$(1+KA-WA)z = PA - PQ + WA \tag{61}$$

We will again remove the displacement due to internal pressure by means of the transformation

$$\overline{z} = z - z_p \tag{62}$$

We now assume that structural damping is proportional to $\overline{z}$, and not to the original variable z. This allows the equation of motion finally to be written in the form

$$\overline{z}^{IV} + (2+WA)\overline{z}'' - g\Omega\overline{z}'(KA)\left|\frac{\overline{z}}{\Omega\overline{z}'}\right| + (1+KA-WA)\overline{z}$$

$$- WA\left(1 + \frac{PA}{1+KA}\right) = -P\Theta \tag{63}$$

It may be seen that this problem may be handled within the same framework as the viscous loss problem but now the loss coefficient c must be written as

$$c = g(KA)\left|\frac{\overline{z}}{\overline{z}'}\right| \tag{64}$$

In this case, it is seen that it is relatively simple to include the structural damping mechanism as part of the contact patch calculations. Identical calculations to those previously described were performed using this loss mechanism and attempting to set the magnitude of the constant g in such a way that the losses were approximately the same magnitude as predicted by the viscous mechanism. Again two different values of the dimensionless foundation modulus $\overline{k}/\alpha^2$ were used, one value of 350 being approximately representative of normal bias ply tires while the other value of 190 is approximately representative of a Michelin belted tire. Some of the results of these calculations using this structural damping mechanism are given in the succeeding figures.

Figure 11 shows plots of the position of the contact patch as a function of velocity for these two values of dimensionless foundation modulus, and using an identical fixed tire deflection of $\Theta_o = 0.375$ in both cases. The loss mechanism in both of these cases was taken in the form given by Eq. (64). It may be seen that for the tire whose dimensionless foundation modulus is approximately that of a bias ply tire, increasing velocity first
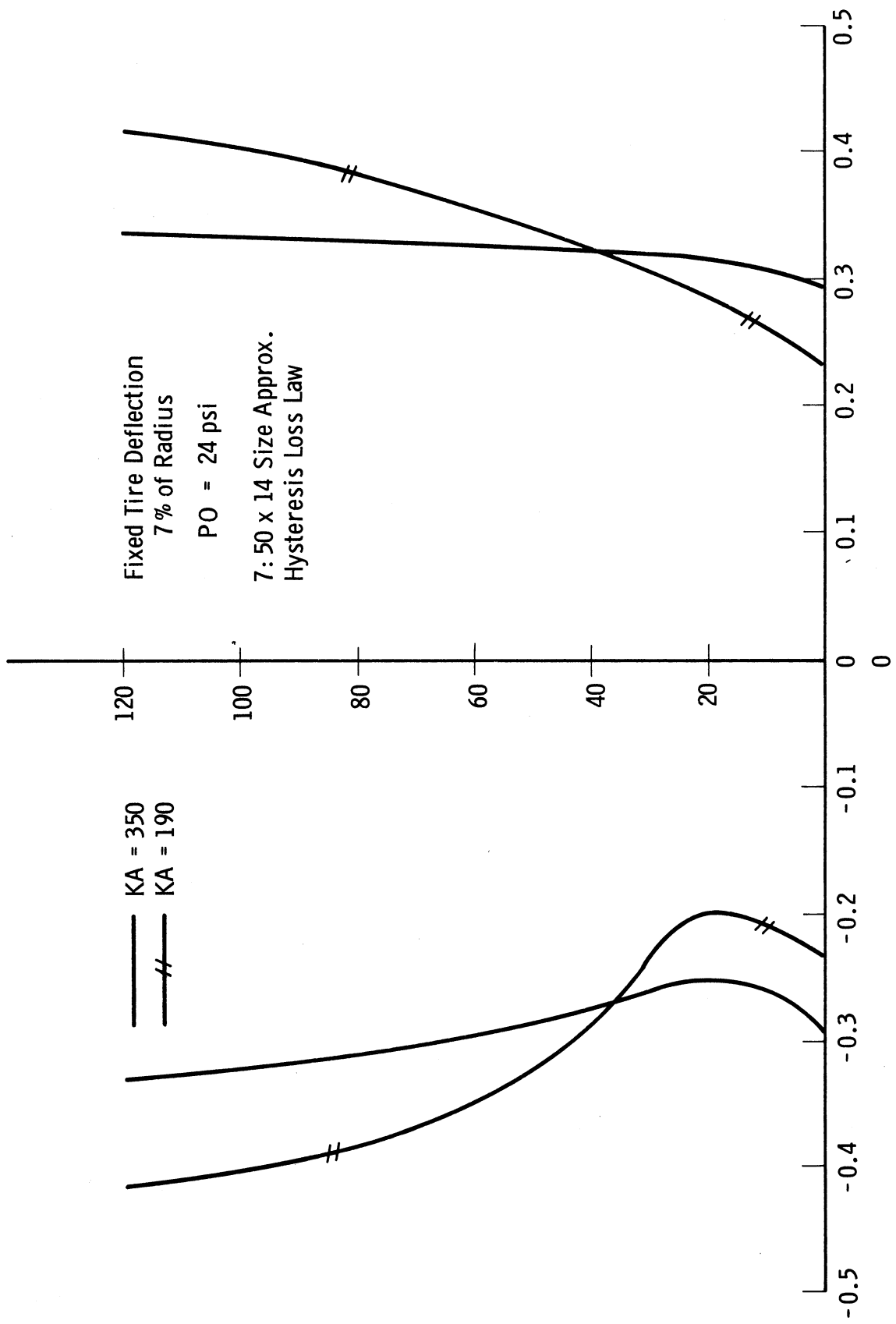
46

Figure 11. Contact patch position vs. velocity.

The figure shows axes with values:

Vertical axis: 120, 100, 80, 60, 40, 20, 0

Horizontal axis: -0.5, -0.4, -0.3, -0.2, -0.1, 0, 0.1, 0.2, 0.3, 0.4, 0.5

Legend:
KA = 350
KA = 190

Text in figure:
Fixed Tire Deflection
7% of Radius
PO = 24 psi
7:50 x 14 Size Approx.
Hysteresis Loss Law

causes the contact patch to move forward and finally to spread out in extent. For the lower value of dimensionless foundation modulus, corresponding to the belted tire, this effect is extremely pronounced and the growth of the contact patch at higher speeds is very noticeable.

In Figure 12 the vertical load carried by two different tires of approximately 7.50x14.00 size is plotted as a function of rolling velocity. The inflation pressure is taken to be 24 psi while the tire deflection is given by $\theta_0 = 0.375$. Again the same hysteresis loss law is assumed for both tires and again two values of dimensionless foundation modulus are compared. Here, it may be seen that the bias ply tire generally increases its load carrying capacity at fixed deflection at a slower rate than does the belted tire. This would seem to indicate that at fixed load the rolling radius of a belted tire would increase more rapidly than the rolling radius of a comparable bias ply tire. The increase in load at fixed deflection for the belted tire is rather remarkable between a speed range of 0 through 120 miles per hour. This is due both to an increase in the contact pressure as well as a considerable growth in the contact patch area.

It should also be noted that the bias ply tire exhibits the rather interesting phenomena of decreasing in its load carrying capabilities up to about 20 miles an hour, at which point its load starts to increase. This is an interesting point and worth comment, since such a phenomena has been observed in laboratory testing on road wheels.

Figure 13 shows the calculated variation in drag force with rolling velocity, again comparing the two different types of tires previously dis-
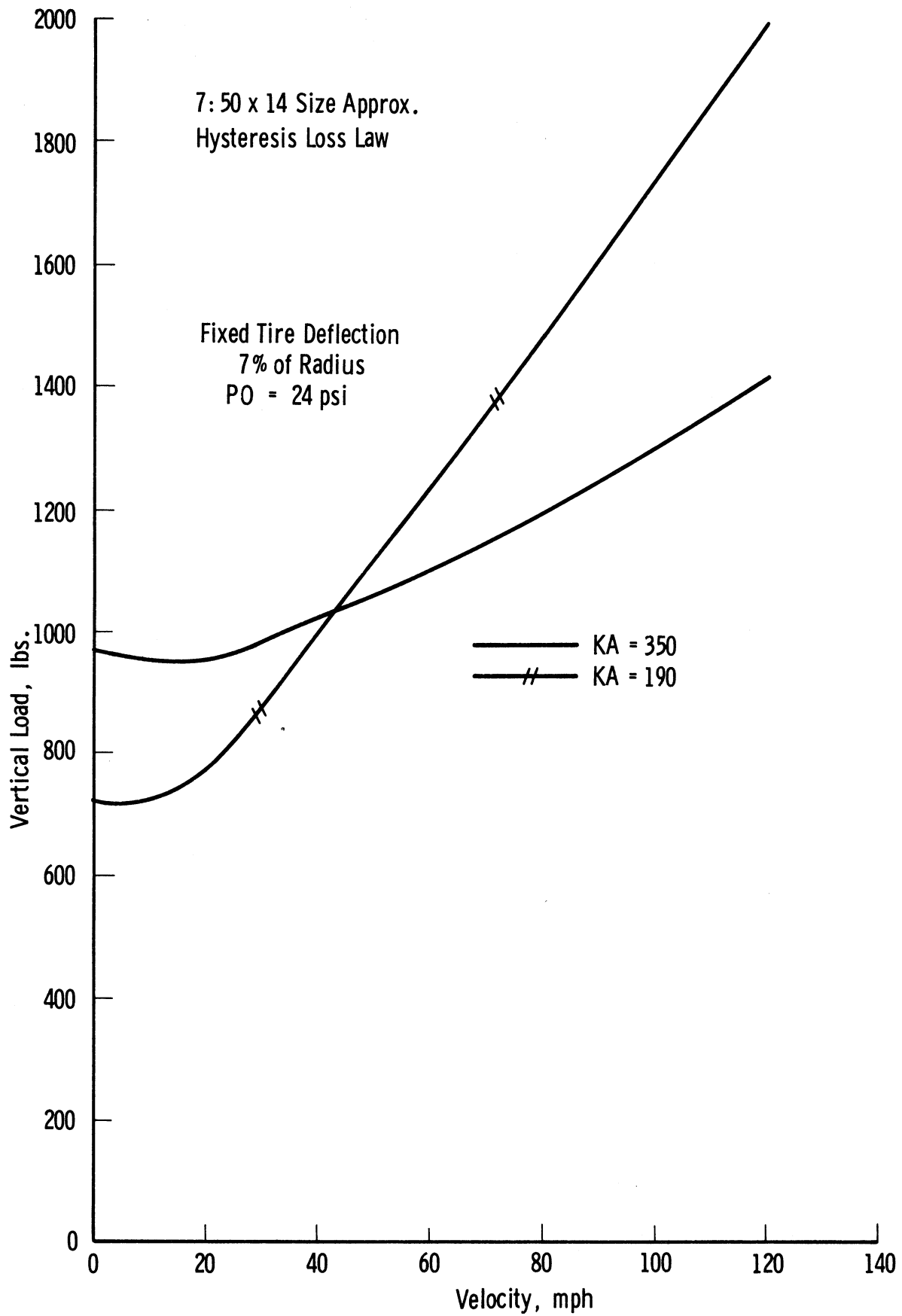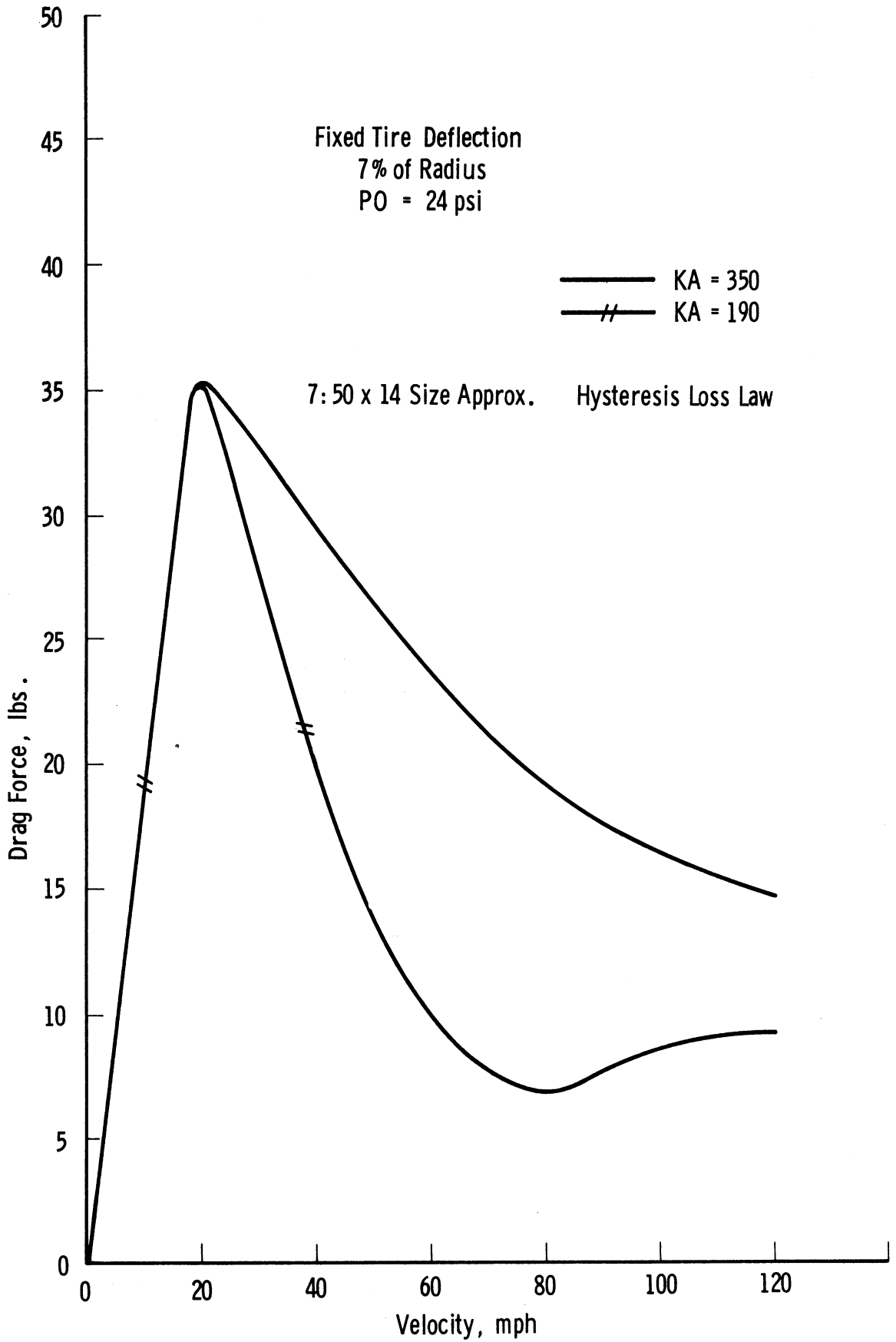
Figure 12. Vertical load vs. velocity.

Figure 13. Drag force vs. velocity.

cussed. The hysteresis loss law seems to predict the drag forces which peak at lower velocities, such as represented here by the 20 mile per hour calculated point, and then decrease as speed becomes greater. This phenomena is clearly represented in Figure 13. As a very interesting feature of Figure 13, one notes that the drag forces exhibited by the particular model representing a belted tire are considerably less for all speeds than the corresponding drag forces for a bias ply tire of the same size, inflation pressure and tire deflection. This seems to indicate that hysteresis loss phenomena predict that the belted tire would be a more efficient tire from the point of view of power consumption. This is in opposition to the result obtained from the viscous damping law, and illustrates the sensitivity of the results to the particular form of loss mechanism chosen for the model.

In the construction of Figure 13, one should not be particularly misled by the fact that the drag forces seem to decrease as velocity builds up. What is important here is the relative drag force between the two tires, and the trends which are indicated. If one were to construct a drag force curve similar to this but using a more exact loss law, say one in which both the real and imaginary parts of the complex material modulus were varied with speed, then one might expect a more realistic representation of the overall drag force as a function of speed. Not much effort has been made here to provide such a realistic law since we feel that the sponsors' own laboratories are much better equipped to formulate such a law than are we.

Figure 14 shows the maximum contact pressure as a function of velocity, again taken for the two types of tires being compared with all other conditions being the same. The inflation pressure is 24 psi in both cases. The static maximum pressure for the belted tire is about 25.5 psi while for the bias ply tire it is about 28.5 psi. As velocity increases, the maximum contact pressure for the belted tire grows more rapidly and at 120 miles per hour it is about 49 psi while for the bias ply tire the maximum pressure at this speed is about 43 psi. As may be seen from this figure, the general trend is for the contact pressure to build up as the tire increases in its rolling speed.

Figure 15 shows plots of the contact pressure distribution versus position in the contact patch for both static and 100 mile per hour rolling velocity conditions. Again, the two types of tires previously discussed are being compared and once again an initial inflation pressure of 24 psi is postulated, along with a fixed deflection corresponding to $\theta_0 =$ 0.375. It may be seen from Figure 15 that for the bias ply tire the initial contact pressures are somewhat higher while the initial contact patch is considerably longer. The combination of these effects causes considerably greater load to be carried by the bias ply tire at zero velocity. As the velocity increases this situation generally reverses and, using this particular hysteresis loss law, it is seen that at 100 miles per hour the pressure distribution for the belted tire now exceeds considerably the pressure distribution for the bias ply tire. Further, the contact patch for the belted tire is now longer with the result that at speed it carries
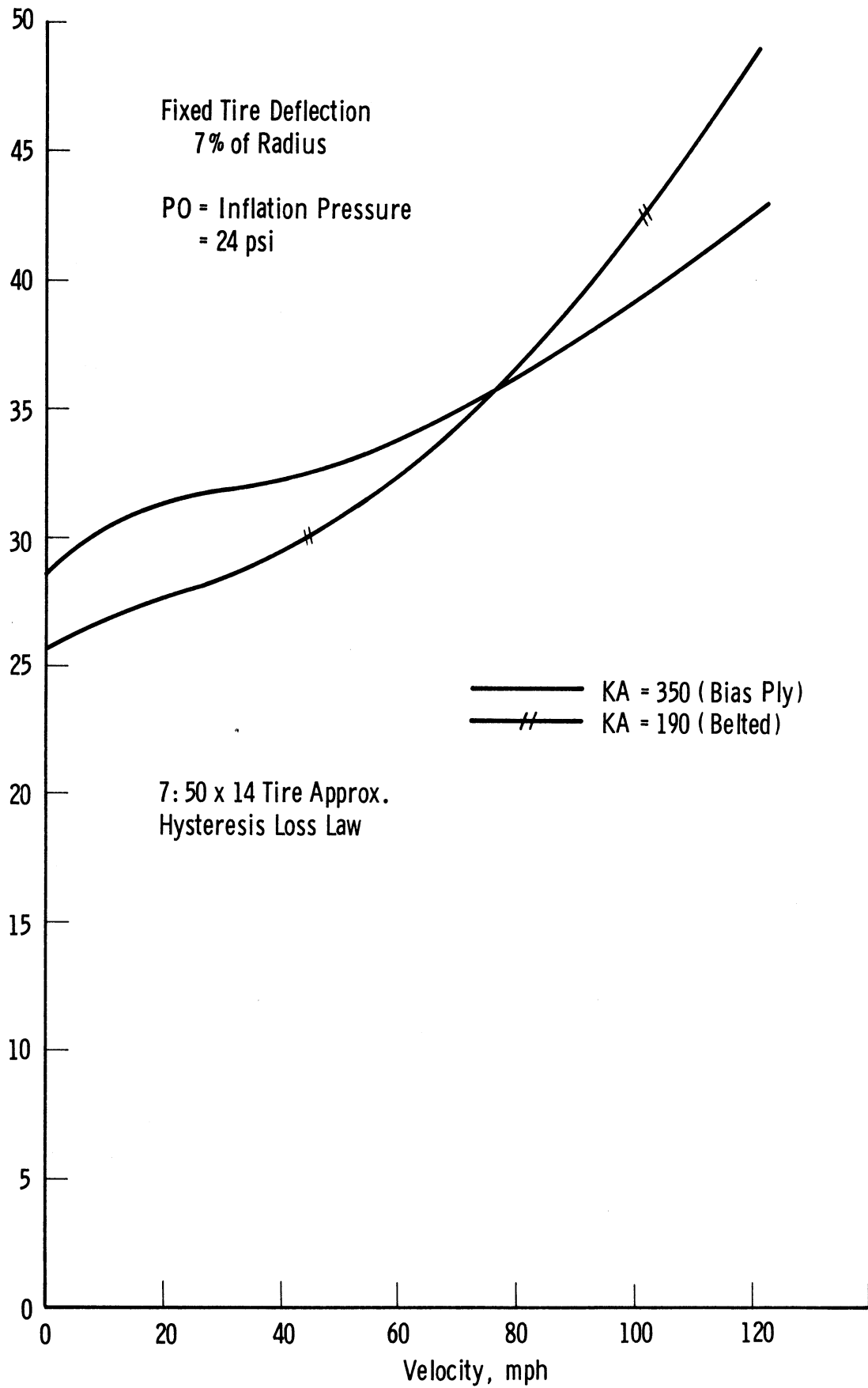
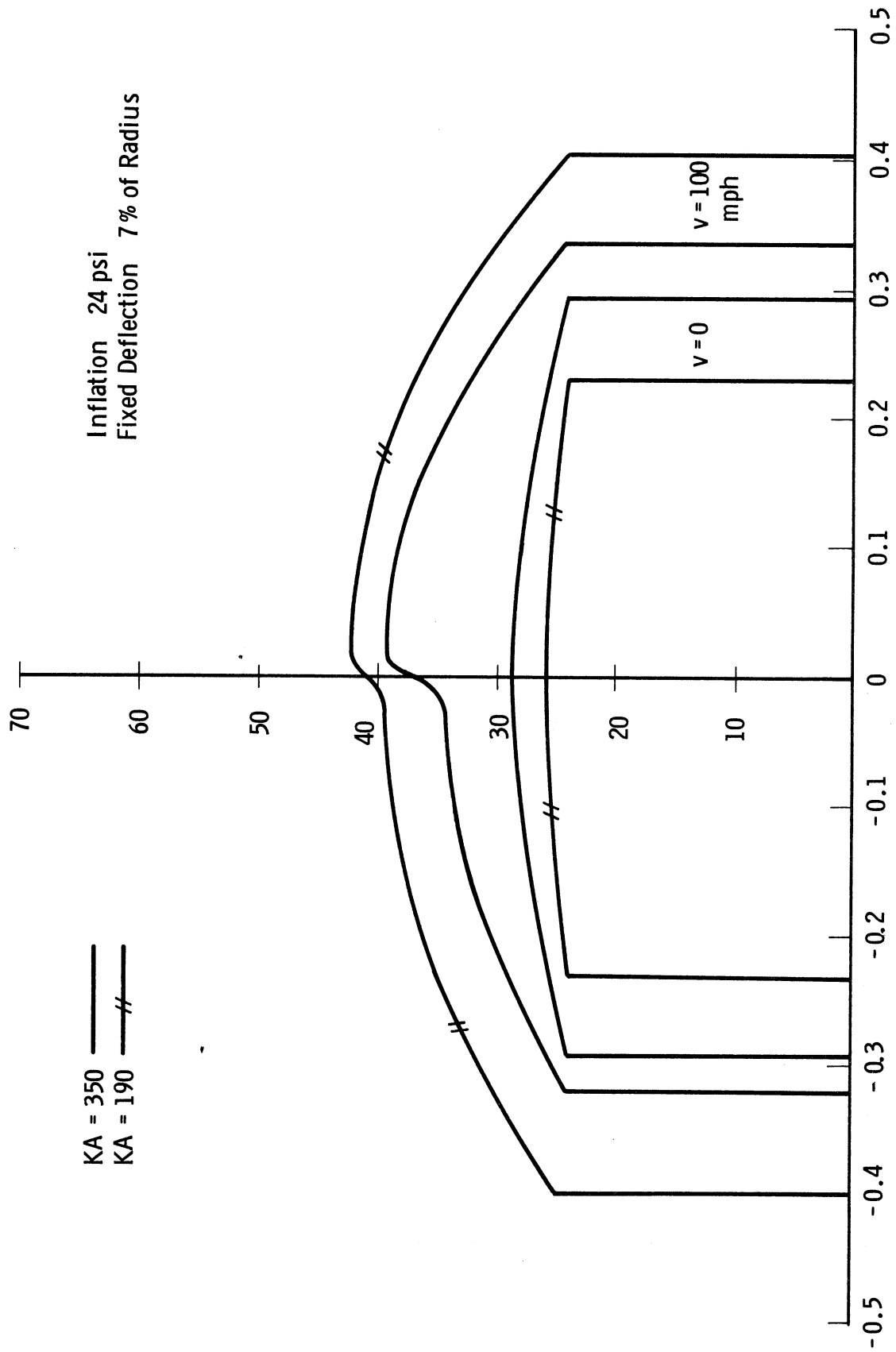Figure 14. Maximum contact pressure vs. velocity.

Figure 15. Contact pressure vs. position for static and 100 mph conditions.

Inflation 24 psi
Fixed Deflection 7 % of Radius

KA = 350
KA = 190

v = 100 mph

v = 0

much greater load than does the bias ply tire. This phenomena of reversal of load carrying capacity seems to be an interesting one and would apparently bear some experimental confirmation.

It should again be emphasized that considerable effort may have to be expended in generating a meaningful loss law for rubber coated fabrics or steel wire used in current pneumatic tire production. However, if this is done, there appears to be a good possibility that a model such as discussed here would well represent many of the phenomena encountered in the straight line rolling of a pneumatic tire under steady state deflection conditions, or under steady state load conditions, where such effects as drag forces, pressure distributions, and load carrying ability are of importance.

VIII. REFERENCES

1. Saito, Y., "A Study of the Dynamic Steering Properties of Pneumatic Tires," 9th International Automobile Technical Congress, 1962, published by the Institution of Mechanical Engineers, London.

2. Thorsen, K. R., 1951 Boeing Airplane Company Report No. D-11719, "A Rational Method for Predicting Tire Cornering Forces and Lateral Stiffness."

3. Clark, S. K. "An Analog for the Static Loading of a Pneumatic Tire," The University of Michigan, Office of Research Administration, Report 02957-19-T. March 1964.

4. Flügge, Wilhelm, "Stresses in Shells," Springer-Verlag, Berlin, 1960.

5. Goodier, J. N. and McJvor, J. K., "The Elastic Cylindrical Shell Under Heavly Uniform Radial Impulse," A.S.M.E. Paper No. 63 APMW-6, 1963.

6. Tong, K. N., "Theory of Mechanical Vibration," John Wiley and Sons, Inc., N. Y. 1961.

IX. DISTRIBUTION LIST

	No. of Copies
The General Tire and Rubber Company Akron, Ohio	6
The Firestone Tire and Rubber Company Akron, Ohio	6
B. F. Goodrich Tire Company Akron, Ohio	6
Goodyear Tire and Rubber Company Akron, Ohio	6
United States Rubber Company Detroit, Michigan	6
S. S. Attwood	1
R. A. Dodge	1
The University of Michigan ORA File	1
S. K. Clark	1
Project File	10